Ultrasonics Sonochemistry 99 (2023) 106581

Contents lists available at ScienceDirect

Ultrasonics Sonochemistry

journal homepage: www.elsevier.com/locate/ultson

Review

Controlling the critical parameters of ultrasonication to affect the dispersion state, isolation, and chiral nematic assembly of cellulose nanocrystals

Robertus Wahyu N. Nugroho [a,b,*], Blaise L. Tardy [c,d,*], Sayed M. Eldin [e,*], R.A. Ilyas [f,g,h,i,*], Melbi Mahardika [a,b], Nanang Masruchin [a,b]

[a] Research Center for Biomass and Bioproducts, National Research and Innovation Agency (BRIN), Cibinong 16911, Indonesia
[b] Collaborative Research Center for Nanocellulose between BRIN and Andalas University, Padang 25163, Indonesia
[c] Khalifa University, Department of Chemical Engineering, Abu Dhabi, United Arab Emirates
[d] Research and Innovation Center on CO_2 and Hydrogen, Khalifa University, Abu Dhabi, United Arab Emirates
[e] Center of Research, Faculty of Engineering, Future University in Egypt, New Cairo 11835, Egypt
[f] Department of Chemical Engineering, Faculty of Chemical and Energy Engineering, Universiti Teknologi Malaysia (UTM), Johor 81310, Malaysia
[g] Center for Advanced Composite Materials, Universiti Teknologi Malaysia (UTM), Johor 81310, Malaysia
[h] Institute of Tropical Forestry and Forest Products, Universiti Putra Malaysia (UPM), Serdang 43400, Malaysia
[i] Center of Excellence for Biomass Utilization, Universiti Malaysia Perlis, Arau 02600, Malaysia

ARTICLE INFO

Keywords:
Cellulose nanocrystals
Ultrasonication
Dispersion
Extraction
Self-assembly

ABSTRACT

Cellulose nanocrystals (CNCs) are typically extracted from plants and present a range of opto-mechanical properties that warrant their use for the fabrication of sustainable materials. While their commercialization is ongoing, their sustainable extraction at large scale is still being optimized. Ultrasonication is a well-established and routinely used technology for (re-) dispersing and/or isolating plant-based CNCs without the need for additional reagents or chemical processes. Several critical ultrasonication parameters, such as time, amplitude, and energy input, play dominant roles in reducing the particle size and altering the morphology of CNCs. Interestingly, this technology can be coupled with other methods to generate moderate and high yields of CNCs. Besides, the ultrasonics treatment also has a significant impact on the dispersion state and the surface chemistry of CNCs. Accordingly, their ability to self-assemble into liquid crystals and subsequent superstructures can, for example, imbue materials with finely tuned structural colors. This article gives an overview of the primary functions arising from the ultrasonication parameters for stabilizing CNCs, producing CNCs in combination with other promising methods, and highlighting examples where the design of photonic materials using nanocrystal-based celluloses is substantially impacted.

1. Introduction

Ultrasound technology is one of the effective techniques to produce a broad spectrum of synthetic and catalytic processes. It possesses a potential use ranging from energy production [1] to food application [2]. There are two categories of ultrasound technology, namely high-intensity and low-intensity ultrasound. They are divided based on intensity and frequency [3–6]. High-intensity ultrasound, denoted as power ultrasound, is characterized by low frequency in the range of 20–100 kHz [5] and high-power intensity of 1–1000 W/cm^2. It further has a destructive characteristic, inciting chemical and physical interactions by producing the implosion of gas bubbles (Fig. 1a and 1c) and microbubble flows [6]. On the other hand, low-intensity ultrasound, also described as diagnostic ultrasound, features an acoustic wave frequency above 1 MHz [5] and an intensity lower than 1 W/cm^2 [6,7]. It is a non-destructive method and demonstrates a weak cavitation impact in

* Corresponding authors at: Research Center for Biomass and Bioproducts, National Research and Innovation Agency (BRIN), Cibinong 16911, Indonesia (Robertus Wahyu N. Nugroho). Khalifa University, Department of Chemical Engineering, Abu Dhabi, United Arab Emirates (Blaise L. Tardy). Department of Chemical Engineering, Faculty of Chemical and Energy Engineering, Universiti Teknologi Malaysia (UTM), Johor 81310, Malaysia (R.A. Ilyas).
E-mail addresses: robe009@brin.go.id (R.W.N. Nugroho), blaise.tardy@ku.ac.ae (B.L. Tardy), sayed.eldin22@fue.edu.eg (S.M. Eldin), ahmadilyas@utm.my (R.A. Ilyas).

https://doi.org/10.1016/j.ultsonch.2023.106581
Received 9 May 2023; Received in revised form 9 July 2023; Accepted 30 August 2023
Available online 3 September 2023

the specified medium, allowing it to characterize and detect the materials of interest [6,7]. Thus, the versatility of ultrasound covers a broad active area of applied frequency specifically applicable and tunable to the number of cavitation events (Fig. 1b) and intensity [8].

This technology further depends on many important parameters during its application in various research fields, including processing volume [12], solvent, and temperature [13]. However, there are three major parameters, thus becoming the most critical parameters that need to be controlled during particle dispersion, namely ultrasonication time, amplitude, and power (or energy). Thus, several interesting papers have reported on the effects of these major parameters on the extraction [13,14] and the dispersion [14–17] quality or coagulation [18] of various products, respectively. In addition to all these fascinating data with ultrasonics treatment, some of its parameters can be adjusted to produce the desired material properties, such as roughness (or topography), particle size distribution, and core–shell structures [8]. However, this has not been synthesized into a review document, which describes and compiles interesting works focusing on these major critical parameters, ultrasonication time, amplitude, and energy input, to control the dispersion state of a nanomaterial obtained from plants.

With the feasibility of altering the physicochemical properties of the material and medium towards the sonication treatment, high-intensity ultrasound is often applied in the following processes: extraction, disruption of cells, emulsification, and modification of crystal structures [19]. Nowadays, the same technology has become a focal point for the dispersion and isolation of nanoparticles, including building blocks such

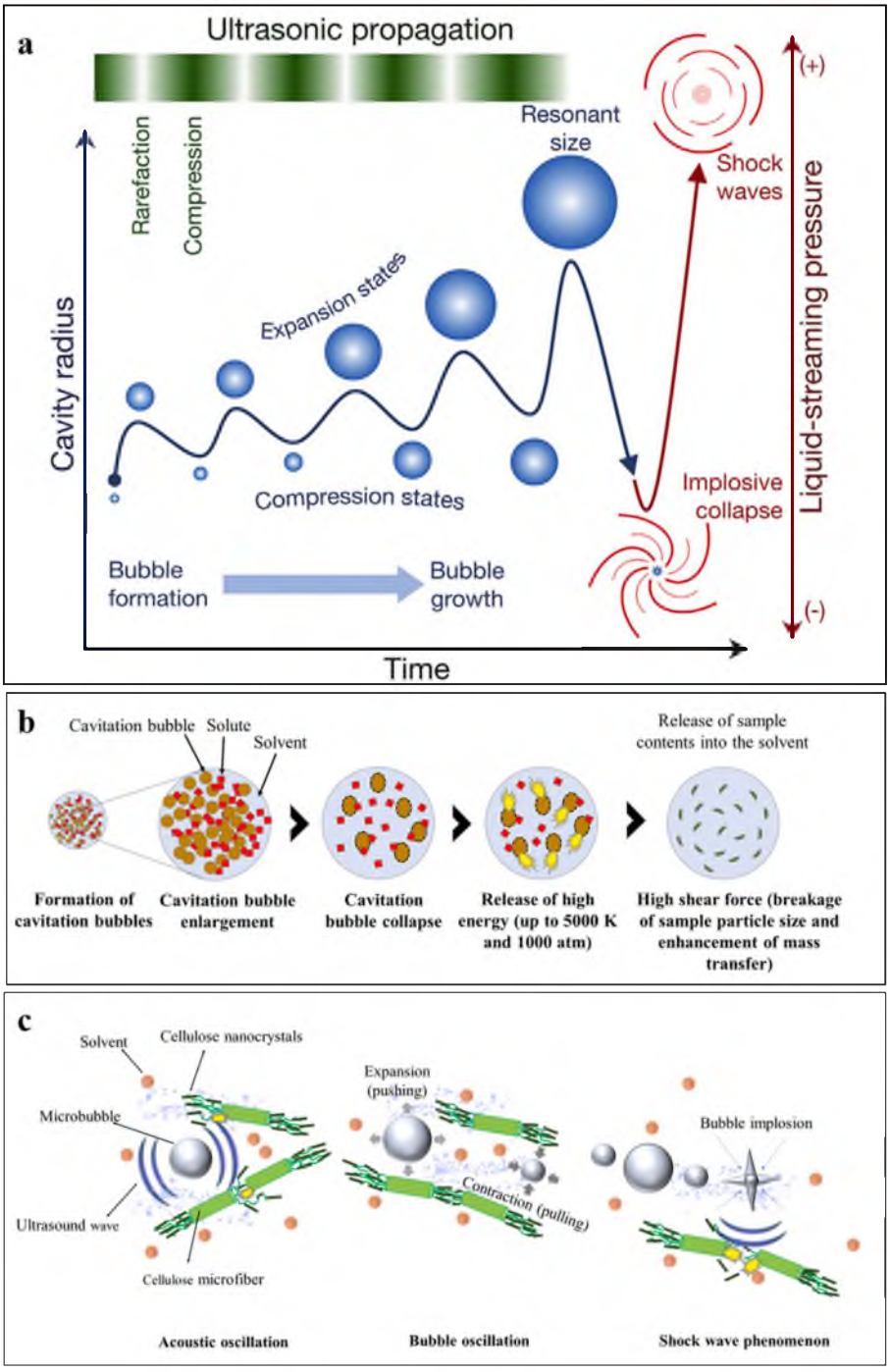

Fig. 1. (a) Illustration of the acoustic cavitation through ultrasonic propagation shock wave after implosive collapse, reproduced with copyright permission from ref. [9], (b) the evolution of acoustic bubbles produced by ultrasonic waves [10], adapted with copyright permission from ref. [7], and (c) isolation of cellulose nanocrystals (CNCs) resulted from the acoustic oscillation of sonication wave, adapted with copyright permission from Creative Commons Attribution Unported License [11].

as cellulose nanocrystals (CNCs), used for the manufacture of sustainable materials.

Cellulose nanocrystal (CNC) or nanocrystalline cellulose (NCC) is a biodegradable, sustainably sourced, and recyclable organic nanomaterial originating from abundant renewable resources on this planet, plants [20]. In addition to the benefits in terms of sustainability, they demonstrate outstanding opto-mechanical properties with a tensile strength ranging between 7 and 8 GPa and an intriguing piezoelectricity [21]. These characteristics have prompted a great interest in fabricating CNC-based products on a larger, commercial, and industrial scale [20]. About their physical properties, they possess a rod-like geometry with a dimension between ca. hundred nanometers up to several micrometers in length and a few tenths in width [22], leading to a highly ordered crystalline phase after the removal of their amorphous parts [23]. Cellulose nanocrystals also have a unique surface chemistry, that depends on the orientation of the crystal planes and the end-groups of cellulose at each end of the nanorods [24–26]. Due to their remarkable properties and nanoscale dimension, CNCs have exhibited tremendous potential applications, such as emulsion, food, composite, cosmetic, medical, and pharmaceutical [27]. However, these cellulose nanocrystals tend to have a concentration-dependent agglomeration [28], since they have broad particle size distributions and an irregular rod-like shape [29]. Nanocellulose may generate percolated fractal networks because of the formation of arrested phases when increasing its concentration. This phenomenon later leads to a shrinking 3D network and reduce the 3D packing spaces between nanocelluloses and eventually, producing random agglomerates [30,31]. Although they are preferable for the transportation of CNC products, a strong drying process reduces their redispersibility. In general, the aggregation-related problem occurs with all nanoparticles due to their high surface area-to-volume ratio [32]. This is more prominent with cellulosic materials, where irreversible aggregation can occur upon drying. Besides that, the CNC polar nature generates compatibility issues, resulting in a challenging process to blend them into non-polar polymeric materials and eventually, leading to poor dispersion and suboptimal physicochemical properties of the composites [33,34]. Thus, understanding the critical parameters of a specific method is highly important to properly control the dispersion state of cellulose nanocrystals and sustain their colloidal stability.

Before controlling its dispersion state, cellulose must undergo a critical process to isolate CNCs from biomass, e.g., plant cell walls, before its use. There are two main pathways to preparing CNCs. The first strategy is mechanical treatment, which include the high-pressure homogenization (HPH) method [35] and high energy ball mill (HEBM) treatment [36]. Compared to ultrasonication, these methods sometimes consume large amounts of energy, thus leading to a high-cost procedure [37]. Then, the second pathway of isolating CNC of various pulps as a raw material is chemical methods involving concentrated sulphuric acid, which is the one conventionally used for a commercial scale due to its simplicity [38]. Most recently, the potential use of ionic liquids (ILs) to obtain nanocellulose is swiftly increasing because of several advantages of these chemicals, like being non-volatile, non-corrosive, and non-flammable [39–41]. In addition, the CNCs produced by ILs demonstrated good thermal stability and high aspect ratios of CNCs [42].

Besides ILs, another chemical method entails the use of deep eutectic solvents (DESs), enabling a sustainable and a simple strategy for isolating CNCs [43]. More importantly, it is a mild extraction process and these solvents can be recycled through a distillation procedure with a recovery rate higher than 85 % [44]. From the extraction standpoint, selective and efficient hydrolysis of the amorphous regions while maintaining the integrity of the crystalline domains is the crucial factor determining a friendly fabrication process of CNCs for the industrial sector [45]. The controlled swelling of cellulose is obtained through the presence of these green solvents, while preventing excessive disintegration of crystalline regions of cellulose [46]. However, the swelling treatment of cellulose is detectable at high temperatures of up to 80 °C by heating [46]. The mass transfer during the extraction process can be thereafter upgraded through a combination of the methods. Hence, the exploitation of ultrasonics treatment [47] in combination with these green solvents, for instance ILs and DESs [48,49] is necessary to improve the accessibility of the amorphous phase of cellulose (Fig. 1c) required for the hydrolytic process to occur at ambient conditions with a low concentration of the solvent [45].

Following the focus on improving the yield of CNC extraction [50,51], the surface charges of the cellulose nanocrystals are a critical parameter for their colloidal stability in water. They also finely control the dispersion state, i.e., primary crystal or agglomerates, the gelation threshold, and the phase transitions into liquid crystalline phase [52–54]. In particular, chiral-nematic (CN) liquid crystals of CNCs form reflective films with reflections tailored to the visible-range, that can be adjusted via ultrasonics treatment [55,56]. Ultrasonication not only increases repulsion between crystals, but also results in more individualized rather than bundled nanocrystals, which can significantly affect the periodicity of the reflective bandwidths present in the CNC films [57–60].

Eventually, this paper aims to provide an overview of the potential use of high-intensity or low-frequency ultrasonics treatment for producing well-dispersed and individualized CNCs. Thus, the first part of this review outlines the critical system configurations, such as time, amplitude, and energy input of ultrasonics treatment, highlighting how these important parameters affect the size, morphology, and other properties of commercial and plant-isolated CNCs, including their yield and stability (Fig. 2a). A combination of ultrasonic treatments and other methods or technologies (Fig. 2b) to extract CNCs will then be discussed while focusing on the effect of these combined methods on the physicochemical properties of CNCs. Finally, the potential ultrasonics treatment to fabricate iridescent and color-controlled solid CNC films from liquid crystalline solutions (Fig. 2c) will be also explored for photonic materials. This latter application is associated with several critical sonication parameters that affects the reflection bandwidth of dried CNC films and other physical parameters covering the isotropic to cholesteric phase transition.

2. The effect of the ultrasonication critical parameters on the stability of CNCs

With several system configurations, ultrasound is an emerging tool to stabilize various oil and organic phases into different aqueous phases in a controlled manner, thus generating homogenous and stable emulsified products [61]. This technology can also be applied to enhance the dispersion state of CNCs in the aqueous systems by disrupting their agglomerated structures. Hence, to obtain stable dispersion, the efficiency of the ultrasonics treatment strongly depends on major critical parameters, i.e., time, amplitude, and sonication energy, which are thoroughly discussed. These three sonication parameters are connected to each other. It is important to note that the effect of these ultrasonication parameters will depend on the original state of the used CNC suspensions. In addition, the CNCs can come from direct isolated samples or commercial samples (hereafter referred to as 'commercial CNCs'). In this section, the ultrasonication is applied to various CNC samples to control their colloidal stability, later displaying the evolution of particles from agglomerates/aggregates, bundles, and individual crystallites.

2.1. Time of ultrasonication

The ultrasound leads to breaking down the large agglomerates into the smaller-sized aggregates, resulting in more stable suspension with homogenous distribution of nanoparticles. The ivory-white color or milk suspension was evident at 0 min of ultrasonication (without ultrasonication), which was associated with the agglomerated structures of CNCs isolated from a bleached cotton fabric [62]. Performing ultrasonication for 1 min on this milk-like suspension may reduce the size of

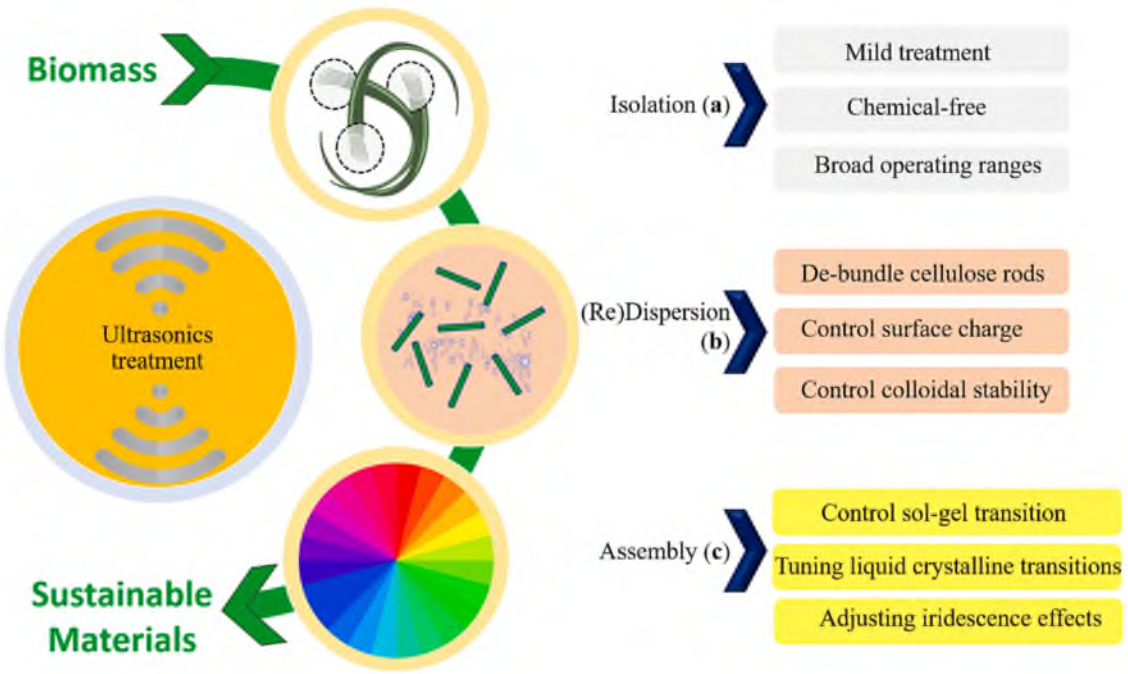

Fig. 2. The application of ultrasonics treatment for (a) isolation (section 3), (b) dispersion (section 2), and (c) CNC-based photonics materials (section 4).

the agglomerated/aggregated CNCs, causing significant changes in the visual observation of the suspension [62]. Thus, ultrasonication time has important effect on the colloidal stability of CNCs. Because of the higher energy input and longer the sonication time, the more dispersed the nanoparticles are. Using the same energy input, the prolonged ultrasonication, i.e., 10 min, resulted in a more homogeneous CNC dispersion than sonicating the same samples for 7 min [17]. Besides controlling long-term stability of CNCs, ultrasonics treatment sustains the surface charge of the CNC suspension. The charged CNC surfaces were still below −30 mV, as obtained through zeta potential measurements, even with a much longer sonication time than 10 min [63]. This case indicates that a sharp decrease of zeta potential up to – 42 mV could be obtained by ultrasonication [63]. This phenomenon could be further related to the partial oxidation of the particles [63,64] through the following mechanisms, previously applied to elucidate the same phenomenon in the crystalline inorganic particles [65], firstly, oxygen gas may exist due to an increase in the number of fine bubbles obtained from the ultrasound [65]. As a result, the contact area of the gas, i.e., oxygen, bubbles, and the liquid medium increases, later promoting the formation of radical species, i.e., $O_2^{\cdot-}$ and $OH^{\cdot}$ [65,66]. Eventually, the interactions between the surfaces of cellulose nanocrystals and cavitation-generated oxygen radicals are unavoidable, generating partial oxidation of nanoparticles and forming more negative surface charges [63]. The nature of these functional groups remains to be elucidated considering the synergistic effect of surface charge and aspect ratio of individual CNC particles. For well dispersed systems, their higher surface charge and aspect ratio will result in early gelation of the solutions, preventing formation of tightly packed liquid crystals (further described more in Section 4) [52,67]. In addition to the surface charge, for example the sulfate moiety, its presence at the nanocellulose backbone is subjected to slow hydrolysis, however, this process could be later accelerated by heating or ultrasonication [46,68].

The disintegration of the CNC agglomerates/aggregates, isolated from a bleached cotton fabric, was noticeable with increasing the sonication period. As a result of this, the diameter of agglomerated particles (D_{v50}) decreased from 14.7 μm to 3.17 μm, 2.71 μm, and 2.23 μm ultrasonicated for 2, 5, and 10 min-ultrasound, respectively [62]. It is worth noting that smaller particle size ($D_{v10} = 0.7$ μm) could be captured for 10 min-sonication. Comparing the particle size distribution (PSD) of different ultrasound-treated suspensions, it is evident that volume distributions underwent a peak shifting to lower values after performing longer sonication [62]. Besides affecting the distribution of the aggregated sizes, at time <15 min-sonication, >20.6 % of CNCs, obtained from commercial microcrystalline cellulose (MCC, Avicel), were in the range of 50–200 nm in length. At a 5 min-sonication, a lower concentration, i.e., 10.9 %, of CNCs had a length ranging between 100 and 250 nm after centrifugation. When extending sonication time to 15 min, 25.2 % of CNCs had a narrower length distribution of 50–100 nm [69]. Nevertheless, at longer sonication time (10 min), the ultrasonics treatment may give rise to some degradation, as unveiled by many thinner and shorter cellulose nanoparticles [62]. Similar to previous finding [62], another emerging study also demonstrated that increasing ultrasonics duration from 10 to 60 min led to sharply decrease size from 1125 to 321 nm [63].

Following the impact of sonication time on the PSD of CNCs, the morphological evolution of CNCs was also detected for varying time lengths of ultrasonics treatment. For example, at 0 min, the CNCs in suspension formed a dense and large aggregated particles with needle-like shapes, reorganizing in parallel structures [62]. Extending the time to 1 min, less densely packed structures with smaller size appeared and significantly assembled into smaller bundles of CNCs [62]. Even though these bundles of CNCs still existed after 5 min-ultrasound, several cellulose nanowshiskers could also be captured. Regarding cellulose nanowhiskers (CNWs), they seem to have similar morphology to CNCs, yet CNW possess low crystallinity due to mechanical fibrillation [70,71]. However, another article describes that whiskers themselves are defined as cellulose fibers that have grown under controlled conditions, thus forming high-purity single crystals [72]. It may be of relevance to mention that CNW and CNC are at times used interchangeably, even if CNW can be put forward as higher crystallinity particles. In addition to the suspension sonicated for 5 min, the width and length of the whiskers were 21 ± 6 nm and 178 ± 65 nm, respectively [62]. Similarly, Li et al. also observed that 10.9 % of the nanoparticles had lengths in the range of 100 and 250 nm at a 5 min of ultrasound [69]. Later, after sonicating for 10 min, the suspension consisted of not only cellulose nanowhiskers, but also some other smaller fragments [62]. Disregarding considerations of size and morphology, the yield of the cotton fabric-isolated CNCs from the applied ultrasonics treatment was

between 41.9 % and 43.4 % averaging at 42.8 ± 0.6 % [62]. However, these results were lower than that of the commercial CNCs produced by Ishak et al. The resultant CNC showed a yield of 84, 86, and 87 % for sonicating at 10, 15, and 20 min [27].

Crystallinity is often described by the crystallinity index (CrI), which represents the mass ratio of the crystalline material relative to the total dry sample based on the crystallographic two-phase model. Daicho et al. highlighted that for nanocelluloses the CrI values demonstrates strong correlations with the corresponding crystal sizes [73]. As the CrI values of nanocellulose increases, its crystal size also enhances. They further noted that an increase in cellulose crystallinity is also affected by the presence of the cellulose bundles, while a decrease in cellulose crystallinity is related to the impact of cellulose disintegration [73]. Following the results of Daicho et al., Rana et al. recently proved that the CrI is directly proportional to the size of a nanocellulose crystallite. The smaller the crystal size, the lower the CrI. They then proposed that the crystallite size is similar to the coherent volume in the substance for each peak of diffraction [74]. Further, X-ray Diffraction (XRD) reveals that a weak and broad peak in the 2θ region of 22°–25° confirmed changes in the crystalline structures of a mixture of freeze-dried CNCs and poly (vinyl alcohol) (PVA) due to a harsh and prolonged ultrasonics treatment. In addition, the freeze-dried CNCs were extracted from pine wood fibers [17]. A well-defined crystalline peak of CNCs at 22.5° was detected for 4 min-sonication. This phenomenon unveils that aggressive and longer time of the ultrasound had a propensity to break up the structures of CNCs, thus deteriorating their mechanical strength and crystallinity [17]. In other words, with increasing time, the ultrasonication turned into a non-selective treatment, removing both the crystalline and amorphous parts and decreasing the crystalline structures [27]. As shown by several following cases, the crystallinity decreased from 82 % of commercial MCC to 81 % of CNCs at 5 min-ultrasonication [69]. Extending the sonication time to 10 min decreased their crystallinity to 78 % of commercial CNCs. Eventually, the crystalline region of commercial CNCs was only 73 % after applying ultrasonics treatment for 15 min [69].

Similar to the results obtained for freeze-dried CNCs, the crystallinity index (CrI) of cellulose nanoparticles, obtained from Ginkgo seed cells, also changed after sonicating for 60 min. Moreover, a higher energy density promoted to dramatically reduce their CrI values [63]. As observed by Ni et al., a significant decrease was found from the CrI of 72 % of non-sonicated cellulose agglomerates with particle size ranging between 13 and 15 μm to 58 % of sonicated cellulose nanoparticles with particle dimension of 24 ± 1.7 nm [63]. A decrease in cellulose crystallinity could be associated with the intense cavitation forces released by ultrasonication [64]. This treatment may provoke the vibrations of polysaccharide's glycosidic hydroxyl moieties, like nanocellulose, resulting in dissymmetry stretching of C-O-C bonds of pyranose ring and C-H vibrations in both types of glycosidic bonds, α-and β-glycosidic bonds [75]. As a result, it may further cause the cleavage of the glycosidic bonds in cellulosic polymer, due to the cavitation effect [76], and subsequently, collapsed their crystalline regions [27]. Then, in relation to the ultrasonication parameter, it is worth mentioning that by increasing the ultrasonication time, more mixing cycles may be exploitable, later improving the efficiency process [77]. The mixing cycle here refers to particle de-agglomeration process. Thus, longer sonication time with the lower sonication power <600 W [63] improves particle de-agglomeration, achieving a homogenous and reproducible dispersion [77].

2.2. Amplitude of ultrasonication

During ultrasonics treatment, amplitude reflects the distance over which the sonication probe can fluctuate longitudinally. With increasing the sonication amplitude, the intensity of cavitation within the liquid also increases [17]. Like the ultrasonication time, the amplitude is also a crucial parameter, that dramatically influences the properties of the freeze-dried CNCs, including their dimensions. For instance, as the amplitude was adjusted from 60 % to 70 %, the diameter of the CNCs decreased from 21 to 16 nm under the influence of a fixed 20 min-ultrasonication [27]. This result indicated that at a higher amplitude of sonication, a decrease in the particle size of CNCs was detected [27]. This phenomenon could be related to the breakage of fibrillary structures due to the extreme particle agitation [78]. However, the opposite profile was observed for increasing the vibration amplitude from 80 % to 90 %, which subsequently increased the diameter of CNCs from 34 to 39 nm, respectively [27]. The excessive vibration amplitude during ultrasonication seemingly caused the agglomeration between individual nanoparticles via secondary interactions or weak forces [79].

Different from the previous result, more freeze-dried CNC bundles, obtained from pine wood fibers, were still found when applying a 4 min-ultrasonication at amplitude of 60 % and 90, respectively. However, the CNC length decreased from 169 ± 11.8 nm at amplitude of 60 to 151.5 ± 8.9 nm at amplitude of 90 %. Thereafter, the individual CNCs existed at 7 min-ultrasonication at the highest amplitude [17], i.e., 90 %. When adjusting the same vibration amplitude, the aspect ratio and length of the CNCs decreased from 10 to 9 nm and 200 to 143 nm, respectively [27]. Further subjecting CNCs to a higher amplitude also resulted in a lower aspect ratio than their counterpart sonicated at a lower amplitude. Nevertheless, a higher standard deviation (SD) found in an aspect ratio of CNCs confirmed the polydispersity of CNCs, regardless of the amplitude used [17].

Well-defined diffraction peaks at 2θ of 14.8°, 16.8°, and 22.8°, in agreement with the planes of crystal structures of $(1\ \bar{1}\ 0)$, (110), and (200), respectively, were detected for the commercial CNCs during the ultrasonication treatments at various amplitudes, indicating the typical diffraction of cellulose I. This finding confirms no significant changes in the main crystal pattern of CNCs under the influence of ultrasound [27,80]. When increasing the sonication amplitude from 60 % to 90 %, the implosive cavitation force induced a greater impact, gradually disintegrating the MCC, enhancing the breakage of crystalline and amorphous domains, and eventually increasing the crystallinity. Finally, the increment of the CNC yield exhibited the effectiveness of sonication amplitude in the range between 60 % and 90 % [27].

2.3. Sonication energy of ultrasonication

Besides the previous two, another key parameter that plays a critical role in controlling the physicochemical properties of CNCs (particle size, polydispersity, crystallinity index, etc.) is the energy input of ultrasound. When high-intensity ultrasounds are applied, gas bubbles exist in the presence of cavitation forces, and they grow continuously [81]. A large amount of sonication energy is produced from the collapse of these gas bubbles, resulting in a mechanical shockwave that interrupts the hydrogen bonded structures of cellulosic fibers (Fig. 1c). Further, at lower sonication energy, the weak bonds of amorphous cellulosic phase rupture, while the interlayers of cellulose undergo partial disentanglement and partial delayering [81]. Together with the previous effect, at higher sonication energy, the breakage of glycosidic bonds of the crystalline region of cellulose occurs following further particle breakage, thus allowing the defibrillation process to occur [81]. However, non-functionalized nanocelluloses often generate strong hydrogen-bonded structures, leading to bundles [82,83]. Even applying high sonication energy seems difficult to fully separate these cellulosic bundles [76,84,85]. In addition to this case, drying form of cellulose nanocrystals potentially promotes significant van der Waals and hydrogen bonding [86,87], leading to a product that will not redisperse, even with intense ultrasonication [85]. In other words, this phenomenon demonstrates that dispersing never-dried cellulose nanoparticles is in general more challenging than if they have never been dried [85]. Nevertheless, the influence of the increasing sonication energy caused the suspension of CNCs to shift their stage from a not-well-dispersed and not well-

distributed state to a well-dispersed and well-distributed state [77].

The sonication technology transforms electrical power into vibrational energy, releasing the ultrasonic waves into the targeted liquid sample. Mathematically, the sonication energy is directly proportional to amplitude (m), area or medium (m^2), liquid density (kg. m^{-3}), and the vibration frequency (Hz) [88]. Thus, larger oscillation amplitudes per unit time promotes larger high-pressure gradients and eventually results in a greater energy. However, another analytical method, i.e., calorimetry, can also be utilized to calculate the amount of energy conveyed to a liquid medium subjected to a direct ultrasound. The total amount of energy transferred to a suspension not only depends on the applied power but also on the amount of time [88]. Thus, the resultant sonication energy, based on the calorimetric approach, is directly proportional to power (W), temperature (K), time (s), and mass of liquid (g). From these two physical standpoints, it is, thus, obvious that time, amplitude, and sonication energy are connected to each other. Consequently, two colloidal suspensions for example, treated at the same energy for different times can significantly demonstrate different dispersion states and particle size [88].

Following the relation between sonication energy and particle size, an interesting result reveals that increasing sonication energy to about 2 kJ/g_{CNC}, the particle size of the CelluForce commercial CNCs remarkably decreased. The size of these commercial nanocrystals slightly changed at higher sonication energies than 2 kJ/g_{CNC} [29]. Following changes in the particle size of the same commercial CNCs (Fig. 3a), the polydispersity index (PDI) changed with sonication energy in the range of 0–4 kJ/g_{CNC} (Fig. 3b) [89]. At the sonication energy of 4 kJ/g_{CNC}, the PDI of the commercial CNCs decreased with a steeper slope than that of the PDI with a low sonication energy, i.e., 1 kJ/g_{CNC}. It is worth mentioning that PDI (ranging from 0 to 1) is determined to evaluate the homogeneity of the suspension [89]. The lower the PDI, the narrower particle size distribution in the colloidal system. However, PDI remained slightly consistent with an energy input of 4 to 50 kJ/g_{CNC} (Fig. 3b). This finding further indicated that the range of energy input of 4 to 50 kJ/g_{CNC} enhanced the particle homogeneity and dispersibility (Fig. 4a) [89]. Besides that, increasing sonication energy at least to 20 kJ/g_{CNC} resulted in similar viscosity values for all these commercial CNC suspensions.

This phenomenon indicates that a good distribution state had been reached through its suspension homogeneity [77]. Nevertheless, Beuguel et al. confirmed that a sonication energy threshold of 10 kJ/g_{CNC} demonstrated a good dispersion of commercial CNCs without any appearance of large aggregates, irrespective of any volume or geometric effects [91].

In contrast to the previous report [29], another study exhibited that changes in particle size of black spruce-derived CNCs were undetected by applying a sonication energy above 1 kJ/g_{NCC} and longer sonication time than 5 min [92]. In addition, no significant change in the hydrodynamic size of CNCs was also observed at the energy input of 3 kJ/g_{NCC} [92]. Concerning the particle morphology, the CNCs sonicated with an energy of 1 kJ/g_{NCC} had a rod-shaped structure like the same sample treated with a higher sonication energy, i.e., 3 kJ/g_{NCC} [92]. In agreement with the data of Dong et al.[55], sonicating CNC suspension with the energy input > 2 kJ/g_{NCC} had no changes in the particle size as characterized by photon correlation spectroscopy (PCS) [56].

In addition, the increment of energy density followed by extending the ultrasonication time was more pronounced to change the particle morphology from long needle-like to short rod-like nanocellulose particles. Thus, lower sonication energy (E_s < 5 kJ/g_{NCC}) was insufficient to disintegrate the covalent bonds of nanocellulose at time <7 min and at room temperature (RT) [56]. Another study unveils that increasing the sonication energy from 5 kJ/g_{CNC} to 7.5 kJ/g_{CNC} with various pulse cycles: 10 s ON/1 s OFF confirmed difficulties in determining the stability of the commercial spray-dried CNCs in suspension and the homogeneity of the particle size [91].

By applying various levels of sonication energy, the structure of this commercial CNC crystalline phase did not alter significantly. Nevertheless, the energy input of ultrasound greatly affected the intensity of characteristic peaks, representing the impact of the energy on the crystallinity index (CrI) of CNCs [89]. With increasing sonication treatment energy from 0 to 50 kJ/kg_{CNC}, the CrI of these commercial CNCs slightly increased from 82.5 % to 82.7 %, 82.8 %, and 83.1 % [89]. The gentle increment of the CrI was related to the removal of amorphous regions of cellulose by sonication energy [27,93]. However, when increasing the energy above 50 kJ/g_{CNC} [89], the intense physical stresses were more profound to induce particle breakage [69], thus following the collapse of the crystalline structure of CNCs and diminishing the CrI, leading to an increase of PDI due to the presence of smaller particle sizes [89].

Following the particle size, morphology, and crystallinity of CNCs, the sonication energy also affects the viscosity of their dispersions. Initially, the suspension of black spruce-extracted CNCs behaved like gel at a concentration of 5 wt-% and 7 wt-%, respectively, without ultrasonication [92]. Upon exposure to an applied acoustic energy, a decrease in viscosity was evident for the CNC samples at predetermined concentrations [92], inducing liquid crystalline phase transitions [55] (further described more in Section 4). With increasing the sonication energy above 0.5 kJ/g_{NCC}, the gel broke, revealing detectable liquid crystalline domains with a fingerprint pattern, a typical of chiral nematic (CN) structures. Further increase in the amount of sonication energy led to CN structures of CNCs with larger pitches, and a decreased viscosity [92]. From the basis of the investigated results, the sonication energy of 1 kJ/g_{NCC} was sufficient to break any aggregated black spruce-derived CNCs in the system. Beyond this energy level, the trends of viscosities did not actually change their profiles [92].

Apart from all of these, the evolution of particle distribution due to

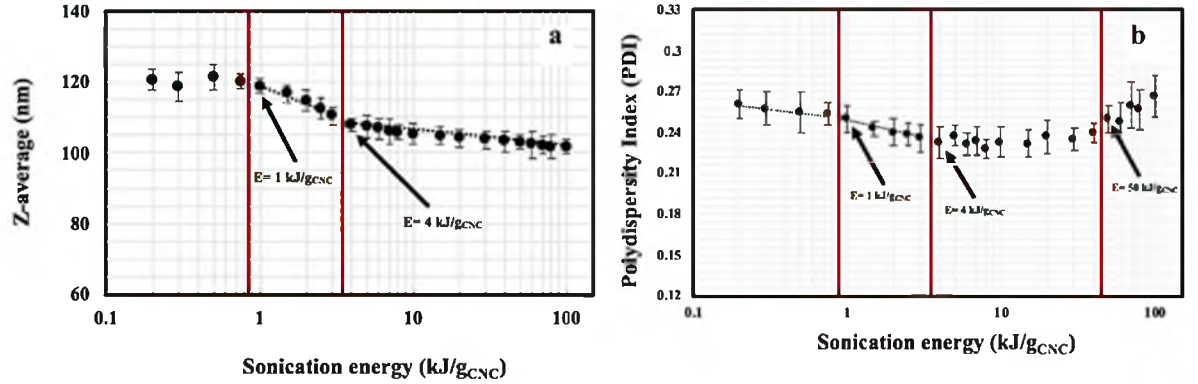

Fig. 3. (a) The effect of ultrasonics treatment on hydrodynamic particle size (Z-average) presented in a logarithmic scale and (b) the effect of ultrasound on polydispersity index (PDI), reproduced with copyright permission from ref. [89].

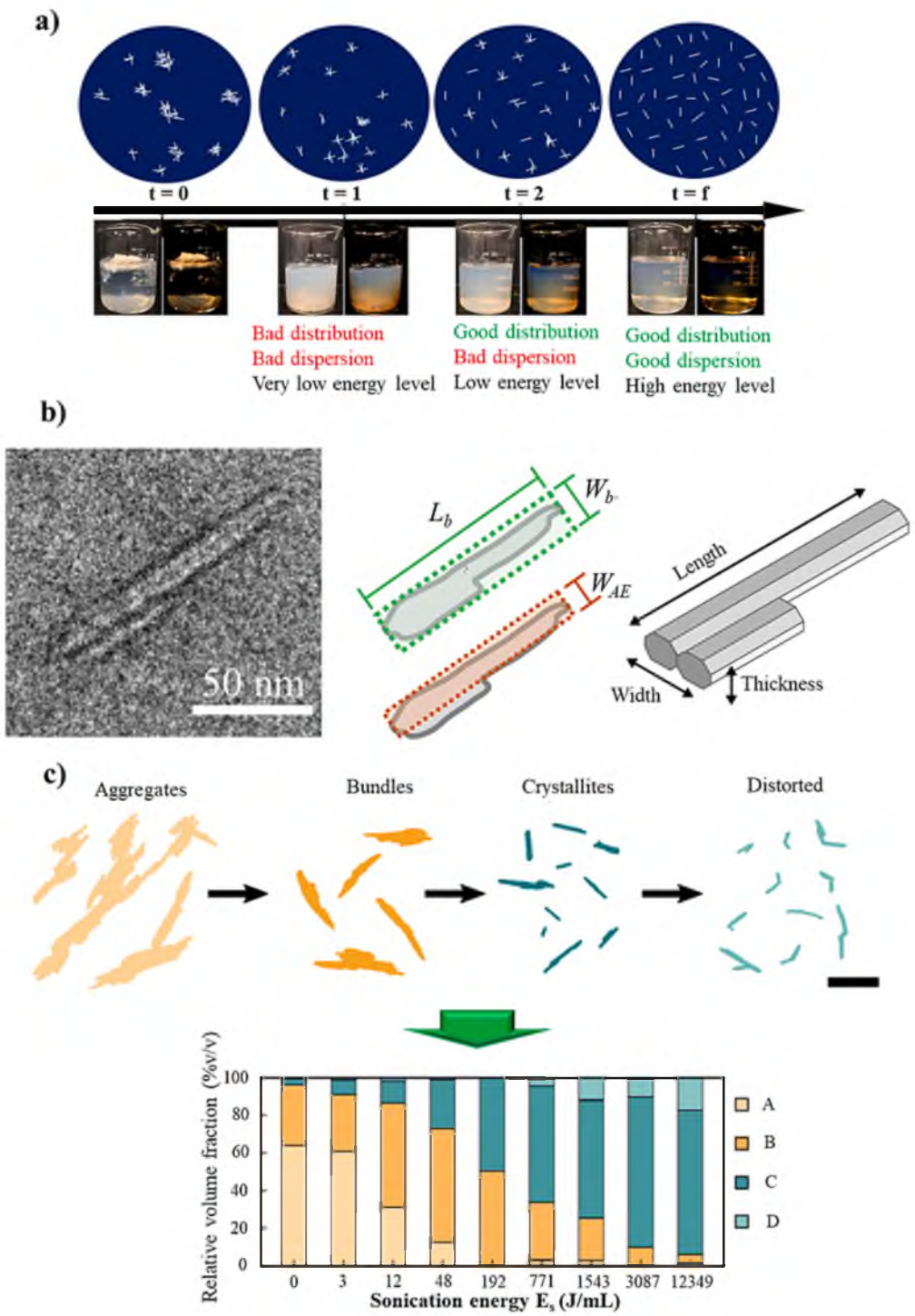

Fig. 4. (a) The dispersion of cellulose nanocrystals (CNCs) under the influence of various level of sonication energies, reproduced with copyright permission from ref. [77], (b) the morphology of the CNC captured by Transmission Electron Microscope (TEM) and the definition of the box width (W_b), box length (L_b), and the width of area-equivalent (W_{AE}), reproduced with copyright permission from Creative Commons Attribution Unported License [90], and eventually (c) the evolution of the sub-populated CNCs and their volume fraction in the suspension when applying various sonication energies, reproduced with copyright permission from Creative Commons Attribution Unported License [90].

the influence of sonication energy was also explored from another perspective [90]. Individual cellulose crystallites possess highly elongated and regular morphology, generating outlines as simple models such as ellipses or rectangles [90]. A simple metrological model allows to quantify the particle size and shape evolution with sonication dose involving the area-equivalent width (W_{AE}) and length (Fig. 4b), displaying the average width of elongated morphology, yet irregular-like particles mainly captured in CNC suspensions. The rectangularity or R lies in between 0 and 1, with R = 1 denoting a particle with an ideal rectangular profile. In addition, it is directly proportional to the W_{AE} profile [90]. The morphology of cellulose particles is further classified based on their threshold profiles defined at $R_o = 0.4$ and $W_{AEo} = 17$ nm. The cellulose nanocrystals demonstrating the width or $W_{AE} > 17$ nm are categorized as composite particles, while the rectangularity profile higher than 0.4 displays a typical of crystallite [90]. Thus, various morphologies of typical cellulose particles can be found out from their measured R and W_{AE}, respectively: (1) distorted crystallites ($W_{AE} < W_{Aeo}$, $R < R_o$), (2) crystallites ($W_{AE} < W_{Aeo}$, $R > R_o$), (3) bundles ($W_{AE} > W_{Aeo}$, $R > R_o$), and aggregates ($W_{AE} > W_{Aeo}$, $R < R_o$). Of note, the bundles are different from the aggregated nanocellulose particles by their disordered morphology, as shown by their rectangularity profiles. This perspective validates that the bundles and aggregated particles populations dominantly appeared upon sonication [90]. During ultrasonication, aggregated particles may undergo significant changes into

smaller structures. However, the bundle-like structures require more high sonication energy to experience breakages into individual crystallites since they are more persistent than the agglomerates.

In some cases, at low energy ($E_s \leq 0.048$ kJ/mL), the ultrasound induced the formation of irregularly shaped cotton fiber with a lower rectangularity tail [90]. The proportion of these irregularly shaped particles quickly decreased with an increase in the energy of sonication. On the contrary, much higher sonication energy ($E_s \geq 0.772$ kJ/mL) led to the development of particles composed of simple crystalline structures distorted by sharp kinks. Even though these kinked particles of CNCs had low rectangularity, they were remarkably thinner than other lower rectangularity particles sonicated at lower sonication energy [90].

In principle, there are interacting forces governing the agglomerates of dried powders, as displayed in Fig. 5, and they include van der Waals force as well as hydrogen-bonding interactions. Conventional drying methods (freeze and spray drying) often result in dense and packed agglomerates of CNCs. The intermolecular hydrogen bonding between hydroxyl functionalities at the nanocellulose surfaces, electrostatic, as well as van der Waals forces between cellulosic hydrophobic sites play a dominant role in various media, including water [31]. Van der Waals and hydrogen bonding are also responsible for cellulose-cellulose cohesion [21,94], and they control the interactions between the hydroxyl moieties and water in the dispersed state [21]. As a result, hydrophobic and hydrophilic parts in nanocellulose are exposed on some facets of the crystals and substantially impact the media interactions, including polymer matrices, organic solvents, or even water [31]. Thus, the ultrasonics treatment tends to weaken these hydrogen-bonded structures, facilitating the (re) dispersion of the cellulosic polymer [31]. However, the cavitation process induced by ultrasonication, as previously mentioned, can break down effectively agglomerated and aggregated particles, resulting into smaller agglomerates and aggregates even individual cellulose nanoparticles [88]. It is believed that the cavitation process of ultrasonication provides extreme temperature gradients and local pressure, resulting in jet streams in few hundred meters per second and strong shock wave [88] (Fig. 1a and c). Consequently, the sonicated particles may collide with each other [88], indicating an increase in the collision frequency between nanoparticles upon ultrasonication [95], surrounded by the collapsing bubbles while allowing localized intense heating and subsequent cooling cycles to occur [88]. Eventually, depending on the effective energy applied to the particles and the thermal properties of the particles, these phenomena can result in re-agglomeration (Fig. 5) or thermally induced interparticle fusion [88]. Following this standpoint, some reports [96,97] have demonstrated that, for some cases extending ultrasonication time for nanoparticle-containing samples provoked particle re-agglomeration, as described in Fig. 5. Similarly, with excessive ultrasonic treatments, aggregated starch clusters seemed to form [98] through secondary or weak forces between the individual particles [79]. The same thing also seems to occur with other nanomaterials, including CNCs under the influence of this excessive ultrasonication.

3. The effects of ultrasonication in combination with other methods for the isolation of CNCs

The potential use of ultrasound in a broad range of applications is related to the presence of cavitation effects (Fig. 1b-c) [8]. The extraction of nanocellulose using ultrasound-assisted methods, including acid hydrolysis, enzymatic hydrolysis, and TEMPO-oxidation has been previously reviewed [11]. Among the other nanocellulose-extracting procedures, acid hydrolysis has been the easiest and the most conventional method for producing nanocellulose from plant-based sources [99]. It is also categorized as the rapid isolation method. The cellulose nanocrystals isolated from this method often possesses smaller sizes up to 4 nm in diameter [100] and 120 nm in length [101]. Here, the acid dissolves and removes the amorphous domain while maintaining the crystalline regions [102]. In the case of producing CNCs with the presence of acid hydrolysis, significant amounts of the acids are abundantly required, which makes this simple method, however, harmful to the environment [103–105]. In other words, highly concentrated acids are equivalent to high corrosive effects [106]. In addition, the acid waste is very difficult to recycle [103], thus causing serious pollution to the surroundings [106]. Further, this acid-related method is often associated with the low process efficiency and the resulting cellulosic products demonstrate a reduction in thermal stability [107].

To overcome adverse effects with the acid hydrolysis method, the isolation of nanocellulose via enzymatic hydrolysis at a pH of 5 and a

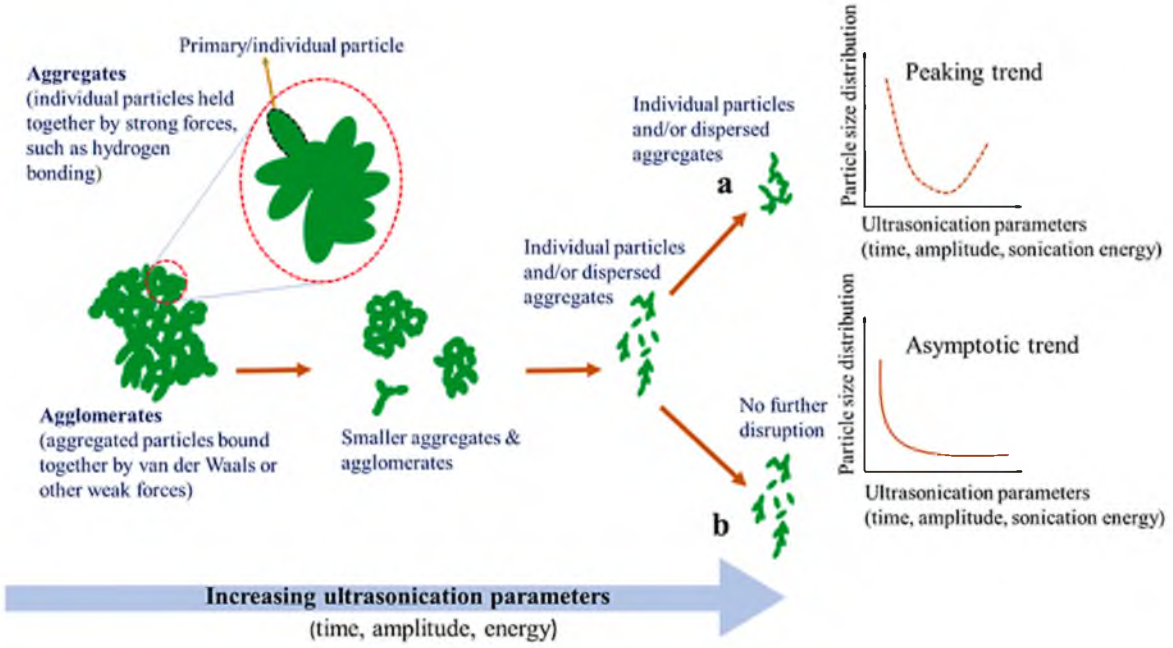

Fig. 5. Schematic illustration of the evolution of various types of particles under the influence of critical ultrasonication parameters, namely time, amplitude, and sonication energy and typical effects of ultrasonication on particle size distribution as a function of ultrasonication parameters, (a) peaking trend (dashed line) vs. (b) asymptotic trend (solid line), adapted with copyright permission from ref. [88].

temperature approximately at 50 °C, respectively, offers less harmful procedures. In addition, this latest method also demonstrates less corrosive and toxic waste [108]. As an example of this treatment, the cellulose nanocrystals with the minimum width of 30 nm and length of 100 nm were successfully captured after applying endoglycanase enzyme [109]. Nevertheless, the enzymatic procedure often requires more time to isolate nanocellulosic particles than the acid hydrolysis method. The first preparation step generally occurs on the scale of days, while the next steps proceed for hours [106,110]. Simply speaking, the procedure is slower than the abovementioned approach. In addition to this approach, the enzymatic hydrolysis is still a costly technology [108].

Eventually, TEMPO-mediated oxidation of CNCs decreases the amount of corrosive chemicals needed for the extraction process. Besides this, the same method tends to modify the surface characteristic of CNCs to facilitate better dispersion in aqueous media [111]. However, the method is also a toxic chemical and a time-consuming method [106].

Yet, other essential isolation methods have not been put forward, such as microwave, ionic liquids (ILs), and deep eutectic solvents (DESs), combined with ultrasonication to isolate CNCs. We herein provide more detailed knowledge on how these latter methods affect the physical properties of CNCs, as the final product and how to produce CNCs with a desirable yield. Thus, this section will provide another perspective on the assistance of ultrasound to promote CNCs extraction using the latter approaches.

3.1. Ultrasonic-assisted microwave treatment

A combined technology such as ultrasonication and microwave has

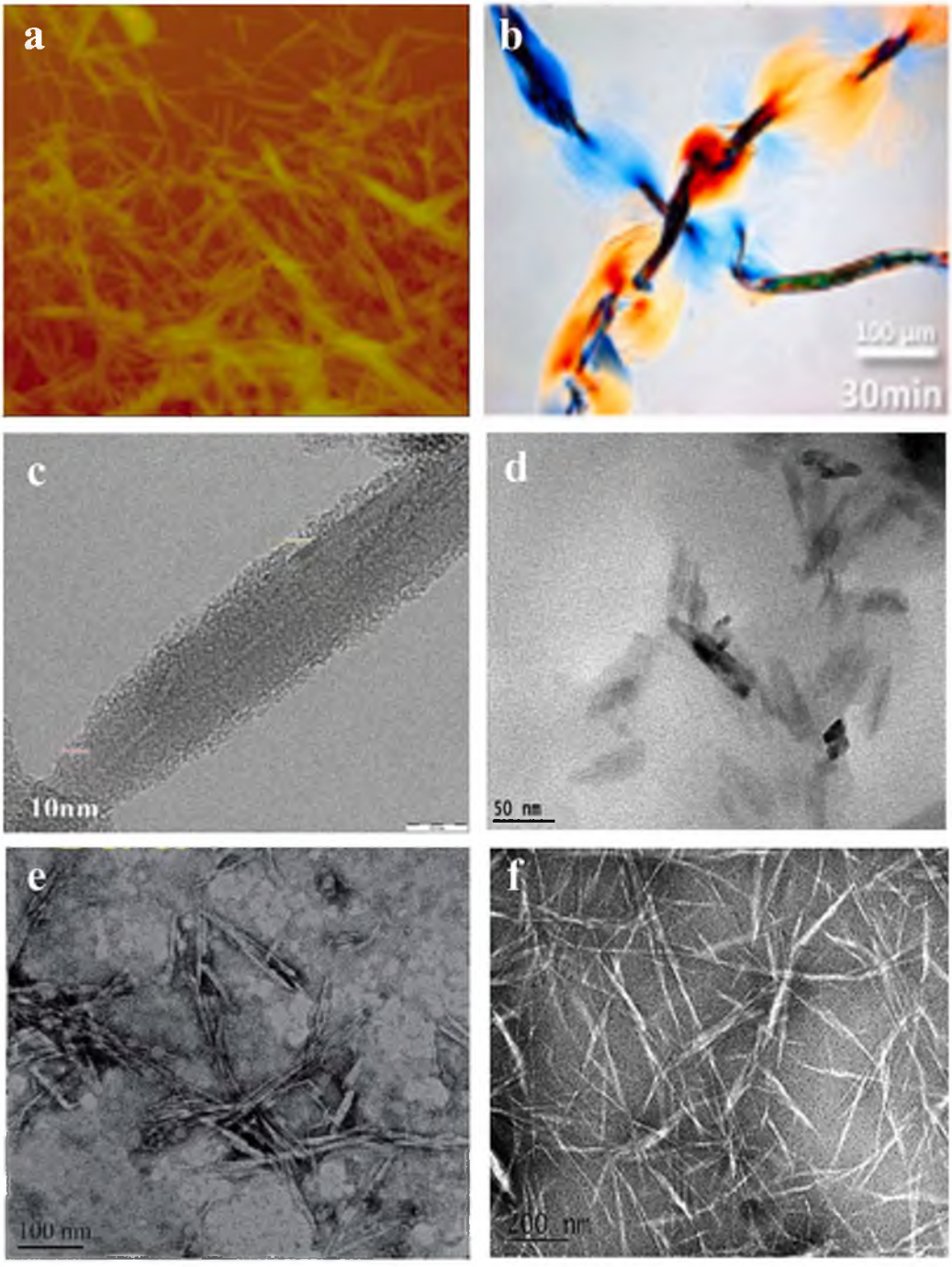

Fig. 6. (a) CNCs produced by ultrasound-assisted microwave, reproduced with copyright permission from ref. [51], (b) totally swollen cellulose fibers after 30 min-treatment with [BMIm]Cl, reproduced with copyright permission from ref. [46], (c) a single CNC with a needle-like shape with a diameter of 21.42 nm, reproduced with copyright permission from ref. [104], (d) CNCs observed at a temperature of 90 °C with an ionic liquid, $[BMIm]HSO_4$, reproduced with copyright permission from ref. [120], (e) the esterified CNCs fabricated by ultrasonic-assisted $[BMIm]HSO_4$ / $[BMIm][BF_4]$, reproduced with copyright permission from Creative Commons Attribution Unported License, [121], and (f) CNCs pre-treated with 30% DES, reproduced with copyright permission from Creative Commons Attribution Unported License [122].

been feasible to activate cellulose fibrils and to obtain optimum fibrillation and hydrolysis efficiency through the intensification of mass transfer and heat [51]. While a microwave source can improve cellulose reactivity and strengthen heat transfer, ultrasound can enhance the efficiency of mass transfer among the cellulose fibers. In addition to this hybrid technology, the microwave radiation absorption generates heat in the entire volume of the substance. The temperature of the material becomes greater inside the material than on its surface, intensifying the mass transfer and heat [112]. On the contrary, high-intensity ultrasound causes the vibration effect, prompting micro vibrations and turbulences near the liquid–solid interface, thus promoting the mass transfer and heat as well [112]. In other words, ultrasonication enhances the mass transfer of the extraction process by producing cavitation-like behavior within the material. When the cavitation bubbles are generated and collapsed, the material cell walls undergo disintegration, and the release of the extracted material is eventually promoted [113]. In fine, the heating effect released by the microwave irradiation is localised in plant cells and its driving force is then combined with the acoustic cavitation of the ultrasonication, triggering the implosion of the plant cell wall to enhance the diffusion of the extracted solute and eventually, the overall rate of mass transfer [114]. Therefore, combining these two technologies in a single-step process would be beneficial to isolate CNCs (Fig. 6a) under mild conditions [51]. During the isolation of CNCs (Fig. 6a), obtained from dried jute stalk, the crystallinity of the sample treated with this combined method increased [115]. The dissolution of the amorphous cellulosic phase occurred along with the removal of hemicellulose. An increase in the sample crystallinity might also be associated with the sample delignification. The cellulosic polymer thereafter exhibited a higher crystallinity index after combining ultrasonication and microwave in the presence of sulfuric acid and ionic liquid [115]. Another result emerged; Lu et al. observed that a rather high yield of CNCs, originated from bamboo pulps, laying between 73.3 % and 80.5 % was gained when keeping at fixed concentration the oxalic acid hydrolysis dosage (15 g acids/g CNCs). The size of the nanocrystals then decreased from 200 to 100 nm when increasing the reaction time from 15 to 60 min [51]. This result was later connected to the nature of microwave irradiation emerging from non-thermal or thermal effects, which was controlled by several critical parameters, such as hot spots, acceleration of ions, heating rate, and rapid rotation of dipoles or collision with other molecules [116,117]. The mass transfer resistance gradually decreased following the hydrolytic cleavage of the glycosidic bonds in the amorphous regions of cellulose [51] under a synergistic effect of ultrasound [118] and microwave [119]. Increasing the acid hydrolysis concentration from 25 to 30 g/g resulted in an increase in the yield from 85.5 % to 77.9 %. Subsequently, a decrease in the size of CNCs was more pronounced from 50 nm to 30 nm. This was ascribed to the fact that the gradual destruction of crystalline structures of CNCs following an increase of acid hydrolysis dosage during the synergistic effect of ultrasonication and microwave, thus allowing carbonization and excessive hydrolysis to occur [51]. Thus, a 25 g/g acid hydrolysis concentration, a 30 min-reaction time, and an 800 W-sonication power, were most favorable to generate high-yield CNCs (Fig. 6a) by combining ultrasonication and microwave synergistically. Of note, the used acid, i.e., oxalic acid, could be reused and recovered for at least five times for producing CNCs [51].

In contrast to the previous study [51], Louis et al. used an alkali treatment in combination with ultrasound and microwave to isolate nanocrystalline cellulose from corn cob [123]. They found out that the yield of CNCs increased to 0.437 g/g when increasing the alkali concentration and sonication time up to 12.5 wt-% and 37.5 min, respectively. However, as the alkali concentration increased further to 20 wt-%, the CNC yield slightly decreased to 0.404 g/g [123]. They later confirmed that microwave assisted bleaching treatment as the first step of the corn cob delignification was better than the pre-treatment with microwave alone. The time consumed for this former treatment was 3.8 times lesser than the latter approach [123]. In addition, the utilized microwave energy during this process was also found to be 4 times lesser than any conventional delignification methods, including H_2O_2 delignification and $NaClO_2$ delignification, as microwave generates direct heating spots and provides a faster reaction rate [123]. Further, ultrasonication helps to break down the holocellulose of corn cob obtained from microwave treatment [123], accelerating the alkaline diffusion and mass transfer, and eventually releasing the CNCs [124,125].

3.2. Ultrasonic-assisted ionic liquid (IL)

Ionic liquids (Ils) are liquid-state organic salts composed of an organic/inorganic anion and an organic cation. They are highly stable with a low melting point, resulting in innovative and sustainable solutions [46,126,127]. Ils are categorizable as green solvents as they do not emit volatile compounds and do not show any measurable vapor pressures [40]. Other advantageous for using Ils as a novel reaction route include their dual role as a catalyst and a solvent, decreasing the reactions steps and additional reagents needed [43].

Interestingly, ILs can be recycled after performing a chemical reaction with the recovery yield approaching 90 % [120,128,129]. In addition, ILs possess several unique characteristics, such as high stability and powerful solvation (Fig. 7). The most well-known strategy of CNCs isolation via hydrolysis in ILs can be divided into several points. Initially, the IL and the cellulose source are mixed and subjected to various reaction conditions [43]. This mixed system is then quenched with an antisolvent, such as water, to precipitate the CNCs. Then, ultrasonics treatment is utilized to eliminate the remaining impurities. After ultrasonication, the precipitated CNCs are gathered separately from their supernatant (antisolvent). Eventually, the supernatant can be evaporated to recollect the IL [43].

The swelling mechanism of cellulose for improving the hydrolysis process was further evaluated [45]. The controlled swelling mechanism of cellulose fibrils (Fig. 6b) was obtained by immersing them in an ionic liquid (IL), 1-butyl-3-methylimidazolium chloride or abbreviated as [BMIm]Cl, while eliminating the dissolution of cellulose crystals obtained from cotton fibers [46]. Interestingly, the combination with ultrasonication had a profound activation effect on the amorphous structures of cellulose. Unquestionably, the selective extraction approaches from the amorphous regions of cellulose could result in CNCs with high crystallinity and yield [45].

Pang et al. studied the possible application of ultrasound into IL pretreatment to enhance the transfer of active species. The width of the commercial microcrystalline cellulose (MCC) was enhanced with a prominent swelling (Fig. 6b) under the influence of ultrasound at a temperature of 45 °C [45]. In addition, the crystalline regions of natural cellulose remained intact after applying ultrasound in [BMIm]Cl, confirming that this technology mainly affected the amorphous domains of the cellulosic polymer. For these IL-isolated CNCs, the crystallinity index (CrI) remarkably enhanced after the selective removal of their amorphous regions [45]. For example, CNCs hydrolysed at 45 °C with a concentration of H_2SO_4 of 21 wt% for 5 h had a CrI of 85.7 % under exposure to ultrasound-assisted [BMIm]Cl. After 5 h-sonication treatment, the size of the crystalline cellulose was highly uniform with a narrow size distribution, indicating a complete release of CNCs from MCC [45]. In addition to size distribution, the diameter and the length of crystals were 22 nm and 240 nm, respectively. Furthermore, after sonication in [BMIm]Cl, the swelling of MCC (Fig. 6b) may happen due to the disruption of the cellulosic glycosidic bonds [104]. A plausible mechanism unveils that $[Cl]^-$ anions originating from [BMIm]Cl attack the cellulosic carbon atoms of the β-1,4-glycosidic linkages. Moreover, $[BMIM]^+$ cations, with its electron rich aromatic benzene ring, also interact with the oxygen atom of the β-1,4-glycosidic linkages through non-bonding π electrons. These molecular level interactions led to the cleavage of the β-1,4-glycosidic linkages within cellulose backbones, further suggesting disintegration of the cellulosic chains [115,130,131].

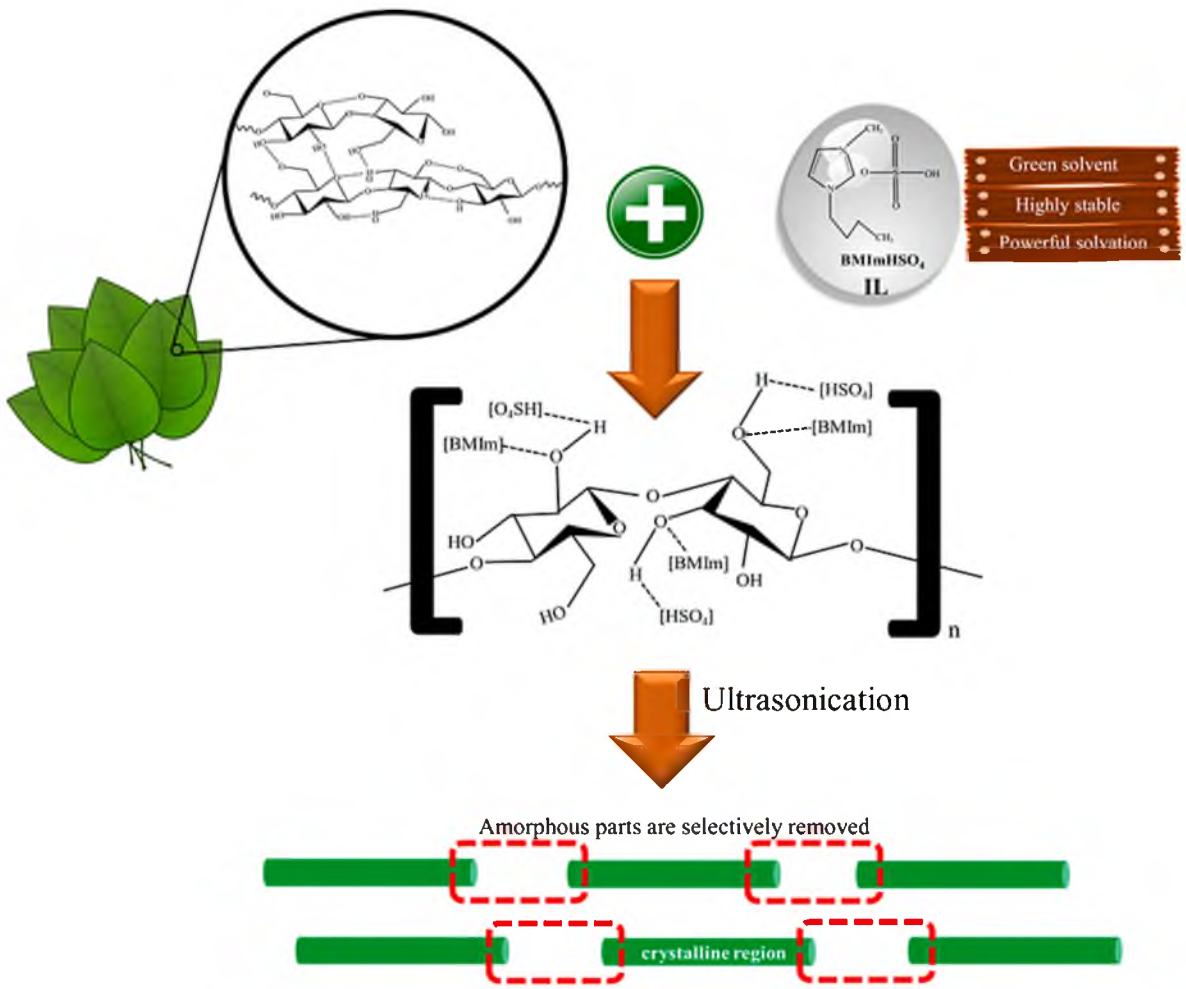

Fig. 7. Illustration of the ionic liquid (IL) benefit for the isolation of CNCs. During the process, the amorphous domains of plant-derived cellulose can be selectively discarded.

Following this mechanism, the water absorption onto the exposed hydroxyl moieties occurred. Hence, the size changed along the longitudinal and width direction due to the effect of swelling [45]. In another study, the CNCs isolated from [BMIm]Cl-mediated hydrolysis under the influence of 5 min-sonication had high crystallinity with a CrI of 88 %. It is most likely due to several factors, firstly, the high crystallinity of the native cellulosic source, cotton gin motes (CGM), used for the generation of CNCs, and secondly, the mild procedures used during nanocellulose extraction [132]. However, as a rule of thumb, the CrI of cellulose nanowhiskers (CNWs) significantly increased with the successive increment of time and sonication power in the presence of IL. The increment of sonication power with the hydrolysis time seems to boost the kinetic force of IL and subsequently improve its diffusion rate inside the amorphous phase of cellulose, obtained from dried leaves of *Adansonia Kilima* (AK) [133]. In addition, increasing the power of sonication may produce more cavitation bubbles allowing the IL to rapidly leap towards the interior of cellulosic matrices and suddenly experience an interior collapse [133] to weaken the hydrogen-bonded structures of cellulose [31]. On the other hand, the enhancement of ultrasonication time may facilitate the mechanism of physical swelling, exposing more surface area for IL to enter and hydrolyse the amorphous region of cellulose, leading to a higher CrI of CNWs [133].

Further, three physical parameters of ultrasound, i.e., power, time, and temperature, play dominant roles in inducing the nanocellulosic yield in ILs. For CNCs originated from CGM, the product was 53 % at 75 °C for 20 h under exposure to ultrasound-assisted [BMIm]Cl and HCl. Then, changing the acid substance to H_3PO_4 decreased the yield of CNCs to 12 % while keeping the power of sonication, time, and temperature constant [132]. Among these variables, temperature was most critically affecting the yield, while the other two variables exhibited a moderate impact. In another study, AK-derived CNCs had the lowest yield when the power, time, and temperature were adjusted to 350 W, 45 min, and 120 °C, respectively [133]. This case thereafter confirms the cellulose disintegration to other liquid fragments rather than producing solid fractions composed of nanocellulose [134,135]. Due to the application of ultrasound-assisted [BMIm]Cl, the CNCs were improved to up to 43 % yield when the reaction time and the temperature were fixed at 44 h and 90 °C, respectively [132]. As a final result of this hybrid method, strong mechanical force originating from a hydrolysing medium of IL and ultrasonics treatment generated defragmentation and defibrillation of long chains of cellulose, leading to CNWs [102].

As observed for [BMIm]Cl, another promising candidate for IL-based isolation of CNCs, obtained from commercial MCC, also produced remarkable results in the form of individual crystals with a diameter of 14–22 nm and a length of 50–300 nm (Fig. 6c) under the influence of an hour of ultrasound [104]. The crystallinity of CNCs during the application of ultrasonication and [BMIm]HSO_4 changed when controlling the temperature of the system [104]. The CrI of CNCs was 91.2 % at 90 °C for an hour of sonication. The CrI was directly proportional to the temperature in the range studied. The lower the system temperature, the lower the CrI of the resultant CNCs (Fig. 6c) [104].

In contrast to a very long period of ultrasound, a 15 min-ultrasound using the same IL, [BMIm]HSO_4 was sufficient to obtain a high degree of cellulose crystallinity at high temperatures such as 90° and 100 °C

[120]. This finding validates the isolation of cotton linter-originated CNCs (Fig. 6d) at high controlled temperatures resulted in more crystalline than amorphous domain as IL or [BMIm]HSO_4 behaves as a chemical agent to selectively remove the amorphous phase of cellulose (Fig. 7) [120]. However, when the system temperature was adjusted to be much higher than 120 °C (maximum point) at different times and ultrasonication power, the CrI significantly dropped [133]. This phenomenon may happen due to the sonication-induced char formation and excessive disintegration of cellulose [136–138]. In another study, higher CrI of CNCs, extracted from cotton fabric, referred to the rearrangement of more crystalline and ordered structures with the presence of ionic liquid [131]. The improvement of degree of crystallinity can be, thus, dealt with the removal and progressive reduction of the amorphous phase of cellulose when increasing the system temperature, making the kinetics of the reaction more favorable [139,140]. Further disintegration of the amorphous cellulose phase made it more feasible to hydrolysis than its crystalline domain [120].

However, the higher temperature seems to induce lower viscosity of IL, which subsequently improves its diffusion rate inside the compact structures of the cellulosic matrices [137]. By increasing reaction temperature and lowering viscosity, hydronium (H^+) ions of IL had more chances to penetrate the amorphous cellulose domain at a higher rate during the acid hydrolysis. As a result, they separated the glycosidic bonds, obtaining individual segments of crystals [140,141]. This study demonstrated that thermo-mechanical effects increased cellulose crystallinity [141]. CNCs extracted at high temperatures, 90° and 100 °C, respectively, exhibited the most refined fibrils, leading to the smaller diameter of fibrillary structures. It presumably indicated a higher aspect ratio of CNCs than MCC [120]. In addition, the effect of high temperature was more pronounced on the product crystallinity. Thus, the CNCs obtained at high temperatures had more crystalline than amorphous parts as the used IL, i.e., [BMIm]HSO_4, was more active at high temperatures, thus selectively removing the amorphous regions. As mentioned, the aspect ratio of the resultant cotton linter derived CNCs was high, approximately 5. The final product of CNCs eventually had a rod-like shape with a length of 75–80 nm and a diameter of 15–20 nm [120].

Another fascinating result reveals that a potential use of binary ionic liquid containing [BMIm]HSO_4 (hydrophilic IL)/[BMIm][BF_4] (hydrophobic IL) in combination with a short time of ultrasound (15 min) led to rod-like shaped esterified-CNCs or E-CNCs (Fig. 6e) with the width ranging between 10–30 nm [121]. In the production of E-CNCs (Fig. 6e), it involved the enzymatic transesterification with the presence of lipase as a hydrolytic catalyst. It, thus, catalyses the transesterification of CNCs with the methyl ester to generate E-CNCs [121]. Compared to the native CNCs, the rod clusters of E-CNCs could exist in some other places and they were separable from each other. It seemed that [BMIm]HSO_4 became a selective liquid to remove the amorphous parts of cellulose, reducing the size of native cellulose from micron to nanometer scale [121]. During the reaction, the hydroxyl functionalities of cellulose experienced a partial substitution, reducing the agglomeration effect and producing well-dispersed E-CNCs. The final product yield of these CNCs, obtained from commercial MCC, was over 78 % [121]. Then, E-CNCs (Fig. 6e) with a degree of substation (DS) of 0.065 had a CrI of 79.89 %, which was higher than that of the same sample with higher DS [121].

3.3. *Ultrasonic-assisted deep eutectic solvents (DESs)*

Similar to Ils, deep eutectic solvents (DESs) are categorized as non-flammable [142], biodegradable [142,143], and green solvents [43,144] since they possess both typical characteristics of organic solvents and Ils. They consist of a mixture of Bronsted or Lewis acid and bases [142]. These solvents originate from the heating of a donor and acceptor pair composed of hydrogen bond capable of generating an eutectic mixture, whereby combined solid salts form a liquid phase [43]. DESs (Fig. 8) have further been attractive for industries and academia because of several advantages, such as ease of fabrication, low-cost, and water insensitivity [145]. The hydrogen-bonded structure of DESs causes it to be a good solvent for different materials as it can compete with other hydrogen bonded systems, including polymeric structures [143,146,147].

To isolate CNCs from cotton fibers (CFs), Liu et al. prepared oxalic acid dihydrate and choline chloride with a molar ratio of 1:1 mixture, which provided a clear and viscous liquid at 80 °C after an hour under reduced pressure [145]. A plausible mechanism of CNCs isolation using DES is that there is a competitive reaction of the hydrogen bonding formation between the hydroxyl moieties in carbohydrates and the chloride ions in DES, weakening hydrogen bonded structures in CFs [145]. Additionally, the oxalic acid solvent has a dissolving power to cellulose glucose and oligosaccharides. Thus, when exposing a microwave-assisted DES to CFs, most of the oligosaccharides, the primary cell wall in cotton, and the partially amorphous cellulose domain undergo dissolution and degradation in this DES, producing some crystalline fragments of cellulose (Fig. 8) [145]. Subsequently, the linkages of microfibers weaken, and their fractions experience a swollen process to get a higher accessibility. Following this phenomenon, ultrasonication plays a dissolution role in separating the CNCs [145]. After this treatment, the surface of the CNCs brings negatively charged carboxyl moieties, inducing a good dispersion in the suspension.

When the suspensions of CFs was subjected to ultrasonics treatment with the power of 1200 W for 30 min, the cavitation force resulting from sonication enhanced the dissolution of CFs fragments, thus producing CNCs [145]. After exposing the samples to this cavitation force, all the suspensions of CNCs had no obvious precipitates. In addition, they also showed colloidal stability apart from the CNCs pre-treated with DES in a microwave at 70 °C. Then, it confirmed the small size of CNCs and the well-dispersed state of CNCs under high-intensity ultrasound [145]. Interestingly, even though keeping similar parameters of sonication, CNCs with various diameters were still observed. Still from the same report, CNCs pre-treated with DES at 70 °C under exposure to a microwave had a diameter of 25 nm, resulting in detectable short fractions intact at the micrometer scale, which might be related to the reaction temperature [145]. Next, cellulose nanocrystals pre-treated with DES at higher temperatures (80° and 90 °C) showed a diameter ranging between 3 and 25 nm. However, the pre-treatment at 100 °C decreased the diameter of CNCs to less than 15 nm. From these results, it has been found out that CNCs could be isolated from ultrasound-assisted DES at temperatures ranging from 70 to 100 °C [145]. It is worth noting that at 70 °C, some agglomerated CFs still existed, leading to the pre-treated CFs with poorly nanofibrillated CNCs, even under exposure to ultrasonics treatment. In addition to all these results, adjusting reaction temperature above 70 °C led to well-nanofibrillated CNCs. Thus, looking from the perspective of energy conservation and high yield, i.e., 74.2 %, the pre-treated CFs at a reaction temperature of 80 °C was an optimal choice to isolate CNCs with this isolation scheme [145].

In another study, increasing the concentration of DES resulted in CNCs, obtained from bleached poplar kraft wood, with a narrower diameter. Further sonicating the suspension for 20 min, changes in diameter size of CNCs pre-treated with 10 % (v/v) and 30 % (v/v) DESs (Fig. 6f), respectively, were found to be insignificant [122]. Yet, the CNCs pre-treated with 30 % (v/v) DES were shorter in diameter (Fig. 6f). Like the previous finding [145], the DES pre-treatment generated negatively charged moieties with carboxyl content in the range of 0.05–0.12 mmol/g on the nanocellulose surfaces [122].

To improve the extraction of CNCs in milder procedures, derivatization of reactive eutectic media has been recently shown to enable a single-step isolation method [43]. The eutectic medium acts as a cellulose-solubilizing agent with its potential ability to form robust hydrogen-bonded structures while introducing the appearance of Leuckart reagent (ammonium formate) to induce the reactivity of the reductive amination of carbonyl moieties existing in the cellulosic

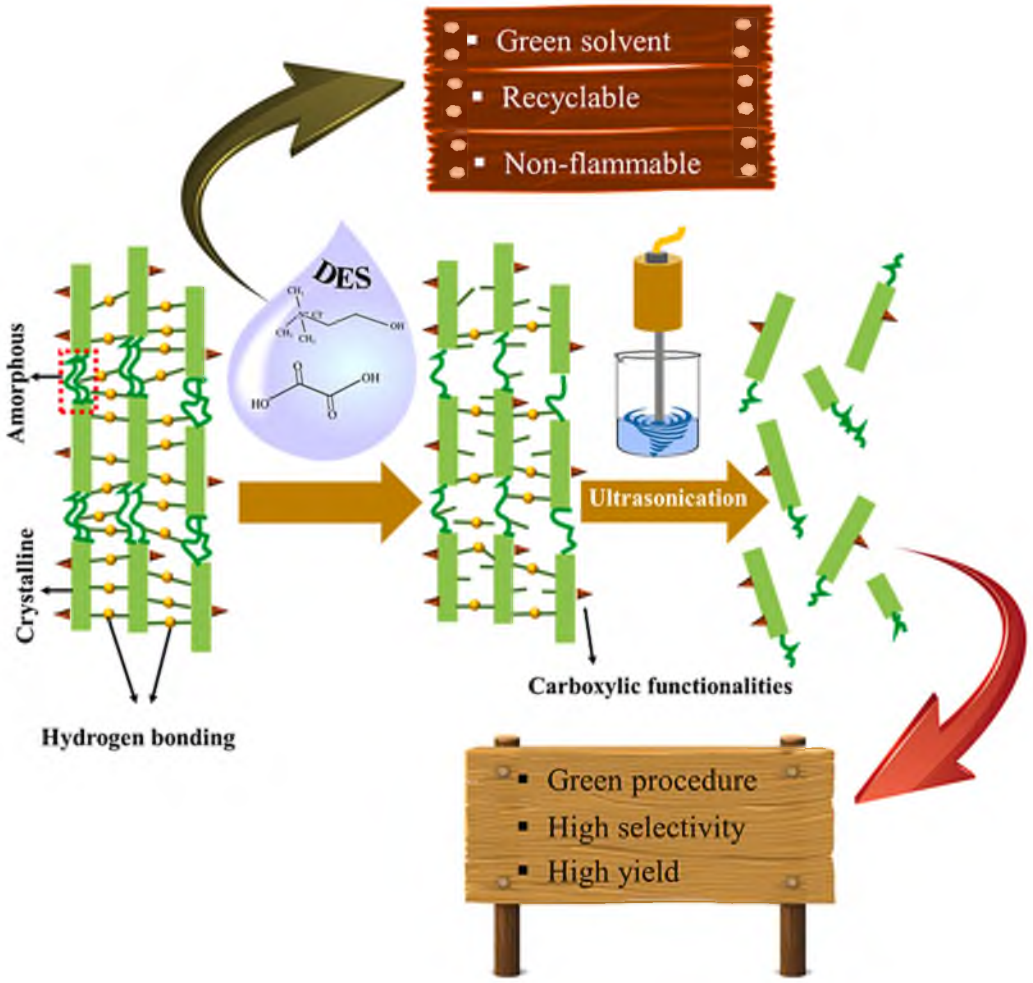

Fig. 8. Schematic diagram showing a benefit of deep eutectic solvent (DES) and its interaction with plant-derived cellulose under the influence of ultrasonication.

linkages [148].

4. The chiral self-assembly of cellulose nanocrystals

Several biological structures are designed with nano-scaled structures to have specific iridescent colors used for signalling, optical protection purposes, or to improve the ability of animals to see [149,150]. Photonic materials composed of chiral nematic (CN) liquid crystals have been widely used in the last few decades to design artificial structural colors based on these fascinating phenomena [151]. Liquid crystals are a state of matter between a solid and a liquid, also referred to as a mesophase [57]. It displays physicochemical properties of a crystalline solid and a free-flowing fluid and birefringence, which depends on concentration or temperature. Birefringence materials possess a refractive index (RI), which is dependent on propagation of monochromatic light and polarization [57]. Liquid crystalline phases (smectic, nematic, and CN) often take on various forms including discs, rods, and plates, among others [57]. For a CN liquid crystal, the selective light reflection at a normal incidence is calculated based on the following equation, $\lambda_{max} = n.P$, where λ_{max}, n, and P are the maximum wavelength of the reflection band, the average refractive index of the solid film, and the pitch, respectively [152,153]. The CN pitch (Fig. 9b), thus, refers to the distance necessary for each layer to complete a 360° rotation around the cholesteric axis [56] (Fig. 9c).

Aqueous stable dispersions of CNCs demonstrate a potential ability to produce a cholesteric liquid crystalline phase, this is a typical liquid crystal with a certain chirality and a helical structure [23,155]. Thus, understanding the self-assembly process of CNCs, particularly the formation of CN, is vital for the design of functional photonic materials [57]. In addition, ultrasonics treatment and CNC concentration play dominant roles in the formation of CN phase (Fig. 9a). The CNC self-assembly requires a critical concentration at the phase transition from an isotropic to an anisotropic [156]. CN assembly occurs from that critical concentration to the gelation concentration where kinetic arrest occurs. This "window" of assembly depends on the dispersion state of CNCs, their aggregation state, aspect ratio, and surface charge [67]. For example, typically, a good dispersion state, with a low aggregation, and small aspect ratio result in higher critical concentration for CN phase appearance and an even higher gelation concentration. Increasing surface charge can result in an early gelation, which reduces the assembly "window" [67]. Critically, all of the key parameters mentioned are affected by sonication treatments, thus presenting an ideal tool to tune chiral nematic phases.

4.1. Effect of ultrasonication on intrinsic properties of phase separated CNCs

In aqueous suspensions, CNCs possess three critical properties that control their phase separation behavior: the surface charge (or charge density), the geometry (aspect ratio and dimension) [56,157], and the electrical double layer (EDL) of the nanocrystals along with their counterions in the aqueous media [56]. In other words, surface charge density, dimensions, aspect ratio, and surface chemistry greatly influence the behavior of phase separation and the nature of the cholesteric

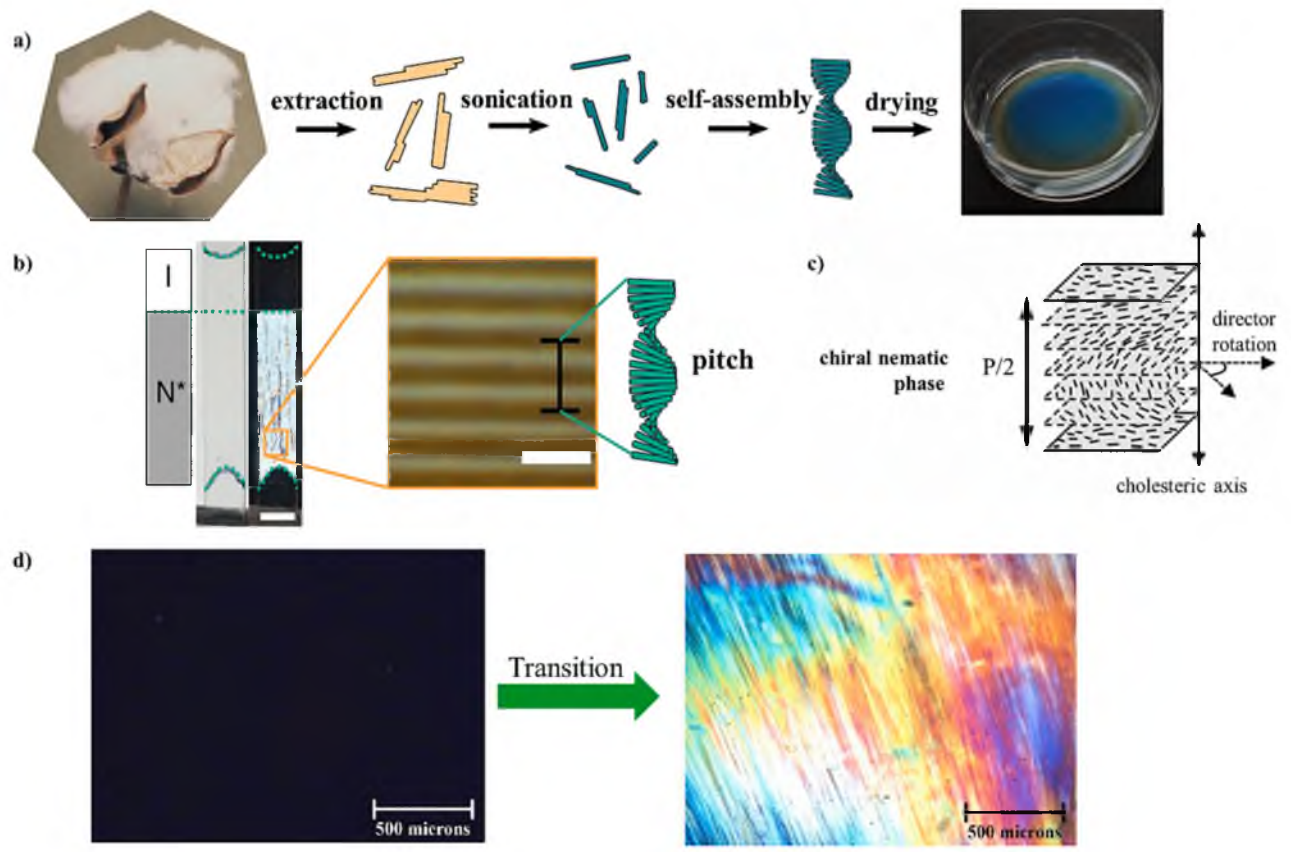

Fig. 9. (a) The production of structurally colored CNC, extracted from cotton, films through chiral self-assembly into a 35 mm Petri dish, reproduced with copyright permission from Creative Commons Attribution Unported License [90], (b) Biphasic phase separation of CNC suspension in a rectangular glass capillary. Vertical separation of this biphasic CNC suspension into isotropic (I) and chiral nematic (N*) phases is obvious when detected using crossed polarisers, as seen in the right photograph, reproduced with copyright permission from Creative Commons Attribution Unported License [90], (c) rotation of the chiral nematic phase around the cholesteric axis with half the chiral nematic pitch, P/2, reproduced with copyright permission from ref. [154], (d) polarized optical microscopy (POM) of spray-dried CNC suspensions sonicated at sonication treatment energy of 10 kJ/g_{CNC} at different concentrations, 3 wt-% (left) and 7 wt-% (right), reproduced with copyright permission from ref. [91].

liquid-crystalline phase [52,158,159]. In addition, the surface charge density of CNCs required to undergo self-assembly in water is in the range of 0.16–0.66 e/nm^2 [151].

For neutral, rod-like crystals, the critical concentrations are dependent on the aspect ratio, i.e., the diameter (or width, D) versus the length (L) [156,160]. Based on experimental studies, the concentration of isotropic-anisotropic transition obtained from the commercial CNC suspensions, CelluForce, has been shown to be 3–4 wt-% [156,161]. Above a critical concentration (c_{crit} ~ 3 wt-%), CNC rods are prone to aggregate and generate ordered structures, commonly called as tactoids, which merge and precipitate to produce an anisotropic phase. Tactoids are defined as liquid crystalline droplets, and they exist in the form of spheres or ellipsoids. These tactoids constitute a transition state between an isotropic liquid and a liquid crystalline behavior (phase separation) [162]. In the homogenous phase, dot-like small tactoids without fingerprint are detected, and when these homogenous tactoids grow or fuse into much bigger clusters, a fingerprint structure (cholesteric behavior) can be captured [163,164].

In relation to the surface charge, if the cellulose crystallites are charged [165], they induce significant electrostatic interactions related to the free energy within the system, allowing the CN phase to form [160]. During sulfuric acid hydrolysis, CNCs abundantly carry residual sulfate moieties that are barely removed. Further, upon the sulfate group ionization, CNCs change into highly charged particles that provoke and stabilize the formation of CN behavior [160]. In addition, the acid hydrolysis leads to protons and residual sulfate ions that strongly interact with the sulfate ester groups of cellulosic polymers, forming the so-called the bound-water layer (BWL) [56]. When the CNC suspensions are sonicated, the input energy may be sufficient to release the trapped ions in the BWL, swell the gel-like layer, and induce the chiral self-assembly of CNCs with a larger pitch length [56].

After ultrasonication, the solvent-casted films from CNC suspensions consisting of longer average length demonstrate red-shifted wavelength in the visible spectrum, while shorter CNCs fabricate films with blue-shifting effect [56]. Further sonicating above ~2 kJ/g_{NCC} did not significantly promote changes in the particle size, while still enhancing the pitch and significantly allowing the optical properties of the resulting films to change as well. This phenomenon indicates that the ultrasonics treatment gives rise to enhanced peak reflection wavelength of iridescent CNC films [56] (Fig. 9d). However, another report unveils that increasing sonication energy may break CNCs into smaller size nanocrystals, thus enhancing the specific surface area and the total number of the particles [159]. Overall, the impact of ultrasonication on aspect ratio is multi-fold, as it can break the clusters of nanocrystals to their elementary size and disintegrate individual nanocrystals into shorter segments along their main axis [90]. Importantly, to date, only sonication was shown to enable de-clustering of CNC bundles as obtained from sulphuric acid hydrolysis [90].

Another interesting paper shows that without ultrasonication, the color of the commercial CNCs films obtained from suspensions had a significantly reduced homogeneity [166] (Fig. 10a, left). Beyond dispersion state, this is as a result of a competition between the energy of packing or assembly and the electrostatic repulsion occurring between particles water evaporation [160]. After ultrasonication, the color

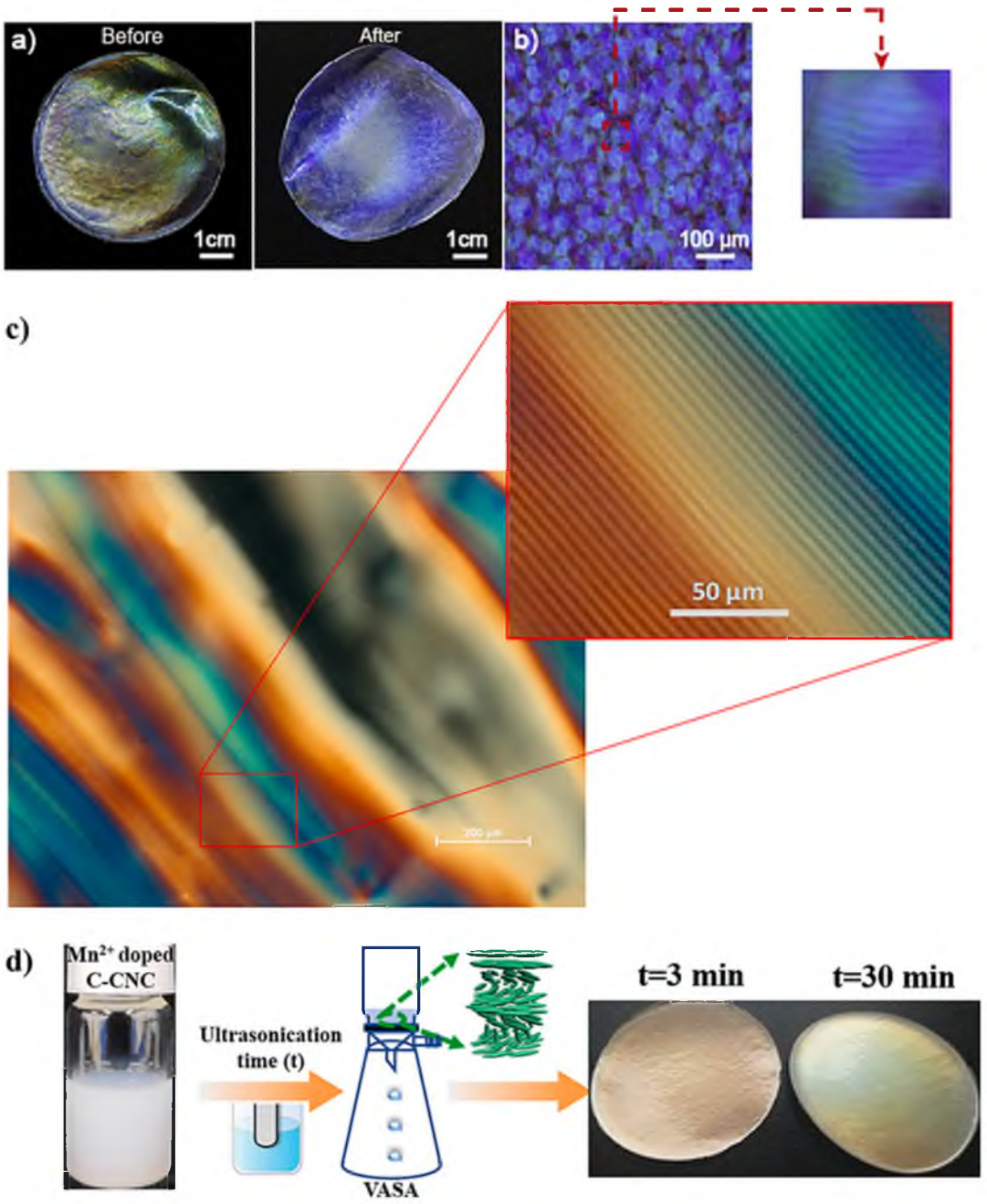

Fig. 10. (a) CNCs containing polycrystalline phase prepared from the suspension before and after ultrasonication. As seen, the color of the solid CNC film before sonication exhibits inhomogeneity. However, the ultrasonics treatment improves a better homogeneity in color, reproduced with copyright permission from ref. [166], (b) a fingerprint image of CNC solid film captured by a polarized optical microscope, reproduced with copyright permission from ref. [166], (c) another extensive fingerprint texture of 5.2 wt-% CNC suspension. The inset displays the fingerprint lines with a spacing of a half pitch, reproduced with copyright permission from Creative Commons Attribution Unported License [168], (d) a scheme of production of CNC structural color via a combination of ultrasound and vacuum filtration technology. Changes in ultrasonication time, from 3 to 30 min, demonstrate an alteration of Mn^{2+}-doped CNC solid film, reproduced with copyright permission from ref. [167].

homogeneity can be more pronounced (Fig. 10a, right), and a fingerprint structure in the films was captured [166] (Fig. 10b). In addition, the photonic properties of solid films (Fig. 9d and Fig. 10a-c) of commercial bleached softwood CNCs may appear mainly due to the tuning of the initially-treated CNC suspensions with high-intensity ultrasonics treatment, causing a red-shift of the reflection wavelength (or band) to occur through the enhancement of the CN pitches in suspensions [56]. The results (Fig. 10d) further reveal vacuum assisted CN phases can be obtained by filtering dilute CNC dispersions, which enables fast formation of photonic reflectors from CNCs [167]. Ultrasonication has been used to disperse highly unstable CNC dispersions in the presence of Mn^{2+} followed by rapid assembly of vacuum assisted self-assembly, which would rapidly aggregate and not form CN phases otherwise [167]. Moreover, due to long sonication time and high power of sonication, some CNCs may rupture, leading to a decrease in their average sizes and causing blue-shifted wavelengths in the resulting films [167].

From another case, the color of the casted CNC films could gradually change from blue to red (Fig. 11a) at various sonication times ranging between 1 and 15 min, later shifting the maximum wavelength from 300 to 700 nm [60] (Fig. 11a). However, at shorter sonication time (<2h), a

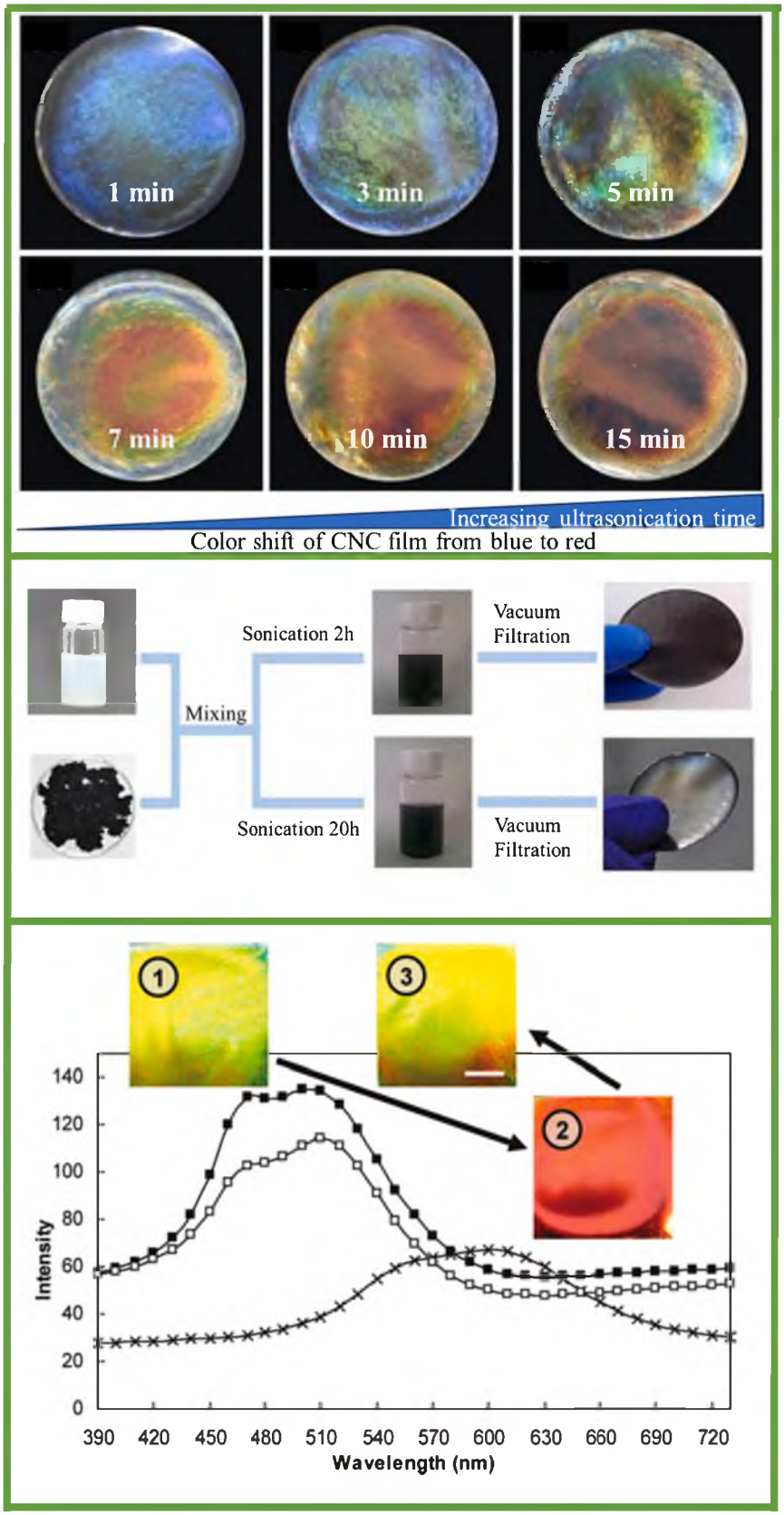

Fig. 11. (a) Pictures of CNC solid films (d = 3.5 cm) treated with various ultrasonication time; reproduced with copyright permission from Creative Commons Attribution Unported License [60], (b) schematic diagram of preparation of thermal reduced graphene (TRG)/CNC composites with or without iridescence, reproduced with copyright permission from ref. [169], (c) reflectance spectra with 45° incidence and detection angles demonstrates the reversibility of salt addition and applied sonication energy to a CNC suspension. Treatments: 1 = 1.2 kJ/g_{NCC} (■), 2 = 1.8 kJ/g_{NCC} (x), and 3 = 1.8 kJ/g_{NCC} + 0.05 wt-% NaCl (□), reproduced with copyright permission from ref. [56].

composite film containing thermally reduced graphene (TRG)/CNCs had no iridescence, whereas, after significant sonication at 20 h, the iridescent color of the composite film was visible (Fig. 11b). The iridescent color of the TRG/CNC films describes that the interaction between CNC and TRG provoking the final self-assembled structure of composite films was altered by ultrasonics treatment [169].

As previously mentioned, EDL can be controlled by the presence of electrolyte. The presence of electrolyte also becomes the key factor in controlling the blue-shift effect caused by the iridescent characteristic of CNCs. The solid CNC, originated from commercial bleached softwood, films composed 0.025–0.4 wt-% NaCl (sodium chloride) had reflective wavelength in the UV and visible regions of the electromagnetic (EM) spectrum [56]. At higher salt concentration, the blue-shifting effect of CNCs solid films was more pronounced at 390 nm [56]. In other word, as higher salt concentration was added into the CNC suspension, a decrease in the P/2 (half CN pitch) was observed, corresponding to a blue-shift wavelength with a smaller λ_{max} [56]. However, increasing the sonication energy from 1.2 kJ/g_{NCC} to 1.8 kJ/g_{NCC} while adding 0.05 wt-% of NaCl (Fig. 11c) exhibited identical output, subsequently validating the red-shifting effect [56]. These phenomena indicate that the reflected colors of the iridescent CNC films can be switched to shorter wavelengths (blue-shift) by increasing the electrolyte concentration in the suspension or to longer wavelengths (red-shift) by increasing the ultrasonication energy [56]. In addition to the blue-shifting phenomenon, this effect is limited by the amount of added salt before the colloidal destabilization of the suspension occurs [165].

In summary, ultrasonication has a multi-faceted effect when it comes to the formation of liquid crystalline phases from commercial and plant-isolated CNCs, respectively. For example, enabling high aspect ratio nanocrystals from their aggregated structures will trigger the formation of liquid crystalline phase transitions of otherwise isotropic assemblies. Then, the same technology can also control the CNC surface charges of which its solution will undergo liquid-crystalline phase transitions before gelation. With the presence of higher charges, an early gelation may occur to prevent the tightly formed liquid crystals. Next, breaking of individual CNC nanorods from anisometric bundles will significantly enhance the aspect ratio, yet diminishing the overall chirality. Hence, going from a simple to a complex process, ultrasonics treatment has been evident to initially induce the appearance of CN characteristics from otherwise isotropically agglomerated/aggregated CNCs. Secondly, the same treatment also causes the breakage of the CNC agglomerates/aggregates, forming CNC with a longer average length with longer pitches and promoting a red-shifting phenomenon [90]. Thirdly, further sonicating CNC agglomerates/aggregates in suspensions may generate shorter CNCs, eventually producing a blue-shifting effect. In addition, extending ultrasonics treatment (>10 h) seems to display a blue-shift wavelength and it could be associated with the surface properties, including surface charges, rather than changes in the CNC size [157]. Overall, when applying the ultrasonics treatment to affect the CNC dispersion and its subsequent assembly into CN materials, one should carefully consider the initial and final state of agglomeration/aggregation of CNCs, the presence of labile functional groups on the surface of CNCs, and whether the treatment would lead to fracture of the individual CNCs. Some broad guidelines can be seen from Figs. 4 and 5.

5. Concluding remarks and future perspectives

A review of the most recent works on various application of ultrasonics treatment for dispersing, isolating, and controlling the structural color of cellulose nanocrystals (CNCs) originating from commercial sources and various plants is presented. Ultrasonics treatment has been favorably affecting the dispersion state of CNCs. Thus, proper ultrasonication parameters (time, amplitude, energy input) should bear in mind to maintain a well-dispersed behavior of these crystalline celluloses for some advanced applications. Further, the ultrasound technology has also been compatible with microwave and other green solvents, i.e., ionic liquids (ILs) and deep eutectic solvents (DES), during the pretreatment stage to isolate this plant-derived nanomaterial. However, most of the studies focused on using ultrasonic-assisted [BMIm]Cl and [BMIm]HSO_4 as ILs and choline chloride (ChCl): oxalic acid (OAD) dihydrate with a molar ratio of 1:1. To reveal the more beneficial application of ultrasonics treatment in the isolation of CNCs with a specific yield, future research should use the hybrid ILs of [BMIm]Cl/[BMIm]HSO4 with different range of molar ratios under the influence of sonication. Further adjusting various molar ratios of natural DESs consisting of ChCl and OAD in combination with ultrasonication should be a fascinating approach to producing a high yield CNCs since by changing the molar ratios between the solvents, new types of solvents with new physicochemical properties are producible.

Besides affecting the stability and the production of CNCs, the adjustment of some critical parameters, for instance, time, concentration, energy input, and combined addition of dilute electrolyte has been feasible to design natural photonic materials consisting of CNCs with unique iridescent colors. In addition, the combination of CNC concentration and ultrasonication, as a function of its energy, contributes to the synergistic effect in shifting the crystalline phase transition of CNCs from isotropic, chiral nematic (cholesteric), and gel-like structures with a preserved CN structure or nematic structures. Nevertheless, there is a lack of detailed protocols focusing on homogenous dispersion of a huge amount of commercial and direct plant-isolated CNCs, respectively, using ultrasonic horn.

As previously noted, commercial CNCs sources are currently available, and they are undergoing large scale-commercialization. This trend has been unimpeded for now almost a complete decade with constant growth. Dried CNCs are typically considerably cheaper due to reduced shipping costs and of other supply chain issues associated with contamination. The price difference is above 10 folds for never-dried or dried CNCs. The main strategy for the (re-) dispersion and breakage of aggregates/agglomerates of dried CNCs is to ultrasonicate them. Therefore, we expect that ultrasound is a promising technology that can be compatible with any other beneficial methods to not only develop the next generation of CNC-based products, but also to further expand the research streams globally from centralized CNC producers. Thereafter, closer interactions between the emerging applied industries and CNC producers can be enabled via a closer industry-academia relationship [170].

CRediT authorship contribution statement

Robertus Wahyu N. Nugroho: Conceptualization, Writing – original draft, Writing – review & editing. **Blaise L. Tardy:** Writing – review & editing. **Sayed M. Eldin:** Funding acquisition. **R.A. Ilyas:** Funding acquisition. **Melbi Mahardika:** Visualization. **Nanang Masruchin:** Visualization.

Declaration of Competing Interest

The authors declare that they have no known competing financial interests or personal relationships that could have appeared to influence the work reported in this paper.

Data availability

No data was used for the research described in the article.

Acknowledgements

This work was funded by the visiting scholar program of National Research and Innovation Agency (BRIN), Indonesia. The authors wish to acknowledge the financial support received from the Future University in Egypt. In addition, we also would like to acknowledge University of Technology Malaysia (UTM) for the project "The impact of Malaysian

bamboos' chemical and fibre characteristics on their pulp and paper properties" [grant number PY/2022/02318 - Q. J130000.3851.21H99]; and the Ministry of Higher Education Malaysia under the Research Excellence Consortium Program [JPT (BPKI) 1000/016/018/25 (57)]. BLT is the recipient of the Khalifa University of Science and Technology (KUST) Faculty Startup Project (Project code: 84741140-FSU-2022-021).

References

[1] B.G. Pollet, The use of ultrasound for the fabrication of fuel cell materials, Int. J. Hydrog. 35 (21) (2010) 11986–12004.
[2] F. Chemat, Zill-e-Huma, M.K. Khan, Khan, Applications of ultrasound in food technology: Processing, preservation and extraction, Ultrason. Sonochem. 18 (4) (2011) 813–835.
[3] A.R. Jambrak, V. Lelas, T.J. Mason, G. Krešić, M. Badanjak, Physical properties of ultrasound treated soy proteins, J. Food Eng. 93 (4) (2009) 386–393.
[4] L. Zheng, D.-W. Sun, Innovative applications of power ultrasound during food freezing processes—a review, Trends Food Sci. Technol. 17 (1) (2006) 16–23.
[5] Z.i. Zhang, D.-W. Sun, Z. Zhu, L. Cheng, Enhancement of crystallization processes by power ultrasound: current state-of-the-art and research advances, Compr. Rev. Food Sci. Food Saf. 14 (4) (2015) 303–316.
[6] X. Fu, T. Belwal, G. Cravotto, Z. Luo, Sono-physical and sono-chemical effects of ultrasound: Primary applications in extraction and freezing operations and influence on food components, Ultrason. Sonochem. 60 (2020), 104726.
[7] I.S. Arvanitoyannis, K.V. Kotsanopoulos, A.G. Savva, Use of ultrasounds in the food industry–Methods and effects on quality, safety, and organoleptic characteristics of foods: A review, Crit. Rev. Food Sci. Nutr. 57 (1) (2017) 109–128.
[8] T.S.H. Leong, G.J.O. Martin, M. Ashokkumar, Ultrasonic encapsulation – A review, Ultrason. Sonochem. 35 (2017) 605–614.
[9] T.Q. Bui, H.T.M. Ngo, H.T. Tran, Surface-protective assistance of ultrasound in synthesis of superparamagnetic magnetite nanoparticles and in preparation of mono-core magnetite-silica nanocomposites, J. Sci-Adv. Mater. Dev. 3 (2018) 323–330.
[10] P. Zhang, Z. Zhu, D.-W. Sun, Using power ultrasound to accelerate food freezing processes: Effects on freezing efficiency and food microstructure, Crit. Rev. Food Sci. Nutr. 58 (16) (2018) 2842–2853.
[11] D.Y. Hoo, Z.L. Low, D.Y.S. Low, S.Y. Tang, S. Manickam, K.W. Tan, Z.H. Ban, Ultrasonic cavitation: An effective cleaner and greener intensification technology in the extraction and surface modification of nanocellulose, Ultrason. Sonochem. 90 (2022), 106176.
[12] W.u. Li, T.S.H. Leong, M. Ashokkumar, G.J.O. Martin, A study of the effectiveness and energy efficiency of ultrasonic emulsification, Phys. Chem. Chem. Phys. 20 (1) (2018) 86–96.
[13] Z. Kobus, M. Krzywicka, A. Pecyna, A. Buczaj, Process efficiency and energy consumption during the ultrasound-assisted extraction of bioactive substances from hawthorn berries, Energies. 14 (2021), 7638.
[14] N. Amiralian, P.K. Annamalai, P. Memmott, D.J. Martin, Isolation of cellulose nanofibrils from Triodia pungens via different mechanical methods, Cellulose 22 (4) (2015) 2483–2498.
[15] H. Yu, S. Hermann, S.E. Schulz, T. Gessner, Z. Dong, W.J. Li, Optimizing sonication parameters for dispersion of single-walled carbon nanotubes, Chem. Phys. 408 (2012) 11–16.
[16] H.W. Xian, N.A.C. Sidik, R. Saidur, Impact of different surfactants and ultrasonication time on the stability and thermophysical properties of hybrid nanofluids, Int. Commun. Heat Mass Transf. 110 (2020), 104389.
[17] J. Shojaeiarani, D. Bajwa, G. Holt, Sonication amplitude and processing time influence the cellulose nanocrystals morphology and dispersion, Nanocomposites 6 (1) (2020) 41–46.
[18] R.E. Kenari, R. Razavi, Effect of sonication conditions: Time, temperature and amplitude on physicochemical, textural and sensory properties of yoghurt, Int. J. Dairy Technol. 74 (2021) 332–343.
[19] E. Keven Silva, G.L. Zabot, A.A.C. Toledo Hijo, M.A.A. Meireles, Encapsulation of bioactive compounds using ultrasonic technology, in: Ultrasound: Advances for Food Processing and Preservation, Elsevier, 2017, pp. 323–350.
[20] S. Beck, J. Bouchard, R. Berry, Dispersibility in water of dried nanocrystalline cellulose, Biomacromolecules 13 (5) (2012) 1486–1494.
[21] R.J. Moon, A. Martini, J. Nairn, J. Simonsen, J. Youngblood, Cellulose nanomaterials review: structure, properties and nanocomposites, Chem. Soc. Rev. 40 (2011) 3941.
[22] D. Klemm, F. Kramer, S. Moritz, T. Lindström, M. Ankerfors, D. Gray, A. Dorris, Nanocelluloses: A new family of nature-based materials, Angew. Chem. Int. Ed. 50 (24) (2011) 5438–5466.
[23] Y. Habibi, L.A. Lucia, O.J. Rojas, Cellulose nanocrystals: chemistry, self-assembly, and applications, Chem. Rev. 110 (2010) 3479–3500.
[24] R.M. Parker, G. Guidetti, C.A. Williams, T. Zhao, A. Narkevicius, S. Vignolini, B. Frka-Petesic, The self-assembly of cellulose nanocrystals: hierarchical design of visual appearance, Adv. Mater. 30 (2018), 1704477.
[25] F. Pignon, E.F. Semeraro, W. Chèvremont, H. Bodiguel, N. Hengl, M. Karrouch, M. Sztucki, Orientation of cellulose nanocrystals controlled in perpendicular directions by combined shear flow and ultrasound waves studied by small-angle X-ray scattering, J. Phys. Chem. C. 125 (33) (2021) 18409–18419.
[26] K. Heise, T. Koso, A.W.T. King, T. Nypelö, P. Penttilä, B.L. Tardy, M. Beaumont, Spatioselective surface chemistry for the production of functional and chemically anisotropic nanocellulose colloids, J. Mater. Chem. A. 10 (44) (2022) 23413–23432.
[27] N.A. Mohd Ishak, I. Khalil, F.Z. Abdullah, N. Muhd Julkapli, A correlation on ultrasonication with nanocrystalline cellulose characteristics, Carbohydr. Polym. 246 (2020), 116553.
[28] E.C. Demir, A. Benkaddour, D.R. Aldrich, M.T. McDermott, C.I. Kim, C. Ayranci, A predictive model towards understanding the effect of reinforcement agglomeration on the stiffness of nanocomposites, J. Compos. Mater. 56 (10) (2022) 1591–1604.
[29] Z.J. Jakubek, M. Chen, M. Couillard, T. Leng, L. Liu, S. Zou, U. Baxa, J. D. Clogston, W.Y. Hamad, L.J. Johnston, Characterization challenges for a cellulose nanocrystal reference material: dispersion and particle size distributions, J. Nanopart. Res. 20 (2018) 98.
[30] V. Guccini, S. Yu, M. Agthe, K. Gordeyeva, Y. Trushkina, A. Fall, C. Schütz, G. Salazar-Alvarez, Inducing nematic ordering of cellulose nanofibers using osmotic dehydration, Nanoscale 10 (48) (2018) 23157–23163.
[31] L. Solhi, V. Guccini, K. Heise, I. Solala, E. Niinivaara, W. Xu, K. Mihhels, M. Kröger, Z. Meng, J. Wohlert, H. Tao, E.D. Cranston, E. Kontturi, Understanding nanocellulose-water interactions: turning a detriment into an asset, Chem. Rev. 123 (2023) 1925–2015.
[32] Y. Min, M. Akbulut, K. Kristiansen, Y. Golan, J. Israelachvili, The role of interparticle and external forces in nanoparticle assembly, Nat. Mater. 7 (7) (2008) 527–538.
[33] E. Sullivan, R. Moon, K. Kalaitzidou, Processing and characterization of cellulose nanocrystals/polylactic acid nanocomposite films, Materials 8 (2015) 8106–8116.
[34] J.-M. Raquez, Y. Murena, A.-L. Goffin, Y. Habibi, B. Ruelle, F. DeBuyl, P. Dubois, Surface-modification of cellulose nanowhiskers and their use as nanoreinforcers into polylactide: A sustainably-integrated approach, Compos. Sci. Technol. 72 (5) (2012) 544–549.
[35] M. Lee, M.H. Heo, H. Lee, H.-H. Lee, H. Jeong, Y.-W. Kim, J. Shin, Facile and eco-friendly extraction of cellulose nanocrystals *via* electron beam irradiation followed by high-pressure homogenization, Green Chem. 20 (11) (2018) 2596–2610.
[36] K.N. Mohd Amin, P.K. Annamalai, I.C. Morrow, D. Martin, Production of cellulose nanocrystals via a scalable mechanical method, RSC Adv. 5 (70) (2015) 57133–57140.
[37] S. Cui, S. Zhang, S. Ge, L. Xiong, Q. Sun, Green preparation and characterization of size-controlled nanocrystalline cellulose via ultrasonic-assisted enzymatic hydrolysis, Ind. Crops Prod. 83 (2016) 346–352.
[38] L. Zhang, X. Jia, Y. Ai, R. Huang, W. Qi, Z. He, J.J. Klemeš, R. Su, Greener production of cellulose nanocrystals: An optimised design and life cycle assessment, J. Clean. Prod. 345 (2022), 131073.
[39] H. Xie, H. Du, X. Yang, C. Si, Recent strategies in preparation of cellulose nanocrystals and cellulose nanofibrils derived from raw cellulose materials, Int. J. Polym. Sci. 2018 (2018) 1–25.
[40] M.J. Earle, K.R. Seddon, Ionic liquids. Green solvents for the future, Pure Appl. Chem. 72 (2000) 1391–1398.
[41] A. Rathore, S. Sharma, A. Sharma, S.K. Sharma, Evaluation of structure-reactivity correlation of efficient corrosion inhibitor ionic liquids for mild steel in acidic medium, J. Dispers. Sci. Technol. 1–13 (2023).
[42] A.P. Gonçalves, E. Oliveira, S. Mattedi, N.M. José, Separation of cellulose nanowhiskers from microcrystalline cellulose with an aqueous protic ionic liquid based on ammonium and hydrogensulphate, Sep. Purif. Technol. 196 (2018) 200–207.
[43] Y. Tang, H. Yang, S. Vignolini, Recent progress in production methods for cellulose nanocrystals: leading to more sustainable processes, Adv. Sustain. Syst. 6 (2022), 2100100.
[44] H. Wang, J. Li, X. Zeng, X. Tang, Y. Sun, T. Lei, L.u. Lin, Extraction of cellulose nanocrystals using a recyclable deep eutectic solvent, Cellulose. 27 (3) (2020) 1301–1314.
[45] Z. Pang, P. Wang, C. Dong, Ultrasonic pretreatment of cellulose in ionic liquid for efficient preparation of cellulose nanocrystals, Cellulose. 25 (12) (2018) 7053–7064.
[46] J. Lazko, T. Sénéchal, N. Landercy, L. Dangreau, J.-M. Raquez, P. Dubois, Well defined thermostable cellulose nanocrystals via two-step ionic liquid swelling-hydrolysis extraction, Cellulose. 21 (6) (2014) 4195–4207.
[47] F. Zhang, Z. Pang, C. Dong, Z. Liu, Preparing cationic cotton linter cellulose with high substitution degree by ultrasonic treatment, Carbohydr. Polym. 132 (2015) 214–220.
[48] J.A. Sirviö, M. Visanko, H. Liimatainen, Acidic deep eutectic solvents as hydrolytic media for cellulose nanocrystal production, Biomacromolecules 17 (9) (2016) 3025–3032.
[49] Y. Meng, Z. Pang, C. Dong, Enhancing cellulose dissolution in ionic liquid by solid acid addition, Carbohydr. Polym. 163 (2017) 317–323.
[50] M. Qian, H. Lei, E. Villota, Y. Zhao, C. Wang, E. Huo, Q. Zhang, W. Mateo, X. Lin, High yield production of nanocrystalline cellulose by microwave-assisted dilute-acid pretreatment combined with enzymatic hydrolysis, Chem. Eng. Process.: Process Intensif. 160 (2021), 108292.
[51] Q. Lu, L. Lu, Y. Li, Y. Yan, Z. Fang, X. Chen, B. Huang, High-yield synthesis of functionalized cellulose nanocrystals for nano-biocomposites, ACS Appl. Nano Mater. 2 (4) (2019) 2036–2043.
[52] J.P.F. Lagerwall, C. Schütz, M. Salajkova, J. Noh, J. Hyun Park, G. Scalia, L. Bergström, Cellulose nanocrystal-based materials: from liquid crystal self-

assembly and glass formation to multifunctional thin films, NPG Asia Mater. 6 (2014) e80.
[53] D. Gray, Recent advances in chiral nematic structure and iridescent color of cellulose nanocrystal films, Nanomaterials 6 (2016) 213.
[54] B.L. Tardy, B.D. Mattos, C.G. Otoni, M. Beaumont, J. Majoinen, T. Kämäräinen, O. J. Rojas, Deconstruction and reassembly of renewable polymers and biocolloids into next generation structured materials, Chem. Rev. 121 (22) (2021) 14088–14188.
[55] X.M. Dong, J.-F. Revol, D.G. Gray, Effect of microcrystallite preparation conditions on the formation of colloid crystals of cellulose, Cellulose. 5 (1998) 19–32.
[56] S. Beck, J. Bouchard, R. Berry, Controlling the reflection wavelength of iridescent solid films of nanocrystalline cellulose, Biomacromolecules 12 (1) (2011) 167–172.
[57] A. Tran, C.E. Boott, M.J. MacLachlan, Understanding the self-assembly of cellulose nanocrystals—toward chiral photonic materials, Adv. Mater. 32 (2020), 1905876.
[58] M. Giese, M. Spengler, Cellulose nanocrystals in nanoarchitectonics – towards photonic functional materials, Mol. Syst. Des. Eng. 4 (1) (2019) 29–48.
[59] P. Saha, V.A. Davis, Photonic properties and applications of cellulose nanocrystal films with planar anchoring, ACS Appl. Nano Mater. 1 (5) (2018) 2175–2183.
[60] R. Duan, M. Lu, R. Tang, Y. Guo, D. Zhao, Structural color controllable humidity response chiral nematic cellulose nanocrystalline film, Biosensors 12 (2022) 707, https://doi.org/10.3390/bios12090707.
[61] S. Kentish, T.J. Wooster, M. Ashokkumar, S. Balachandran, R. Mawson, L. Simons, The use of ultrasonics for nanoemulsion preparation, Innov. Food Sci. Emerg. Technol. 9 (2) (2008) 170–175.
[62] E. Csiszar, P. Kalic, A. Kobol, E.deP. Ferreira, The effect of low frequency ultrasound on the production and properties of nanocrystalline cellulose suspensions and films, Ultrason. Sonochem. 31 (2016) 473–480.
[63] Y. Ni, J. Li, L. Fan, Effects of ultrasonic conditions on the interfacial property and emulsifying property of cellulose nanoparticles from ginkgo seed shells, Ultrason Sonochem. 70 (2021), 105335.
[64] A.L.R. Costa, A. Gomes, H. Tibolla, F.C. Menegalli, R.L. Cunha, Cellulose nanofibers from banana peels as a Pickering emulsifier: High-energy emulsification processes, Carbohydr. Polym. 194 (2018) 122–131.
[65] Y. Kitamura, H. Okawa, T. Kato, K. Sugawara, Effect of ultrasound intensity on the size and morphology of synthesized scorodite particles, Adv. Powder Technol. 27 (3) (2016) 891–897.
[66] B.H.J. Bielski, D.E. Cabelli, R.L. Arudi, A.B. Ross, Reactivity of HO_2/O_2 radicals in aqueous solution, J. Phys. Chem. Ref. Data. 14 (1985) 1041–1100.
[67] T. Abitbol, D. Kam, Y. Levi-Kalisman, D.G. Gray, O. Shoseyov, Surface charge influence on the phase separation and viscosity of cellulose nanocrystals, Langmuir 34 (13) (2018) 3925–3933.
[68] L. Lewis, M. Derakhshandeh, S.G. Hatzikiriakos, W.Y. Hamad, M.J. MacLachlan, Hydrothermal gelation of aqueous cellulose nanocrystal suspensions, Biomacromolecules 17 (8) (2016) 2747–2754.
[69] W. Li, J. Yue, S. Liu, Preparation of nanocrystalline cellulose via ultrasound and its reinforcement capability for poly(vinyl alcohol) composites, Ultrason. Sonochem. 19 (3) (2012) 479–485.
[70] Q. Wang, J.Y. Zhu, J.M. Considine, Strong and optically transparent films prepared using cellulosic solid residue recovered from cellulose nanocrystals production waste stream, ACS Appl. Mater. Interfaces. 5 (7) (2013) 2527–2534.
[71] H. Wang, J.J. Zhu, Q. Ma, U.P. Agarwal, R. Gleisner, R. Reiner, C. Baez, J.Y. Zhu, Pilot-scale production of cellulosic nanowhiskers with similar morphology to cellulose nanocrystals, Front. Bioeng. Biotechnol. 8 (2020), 565084.
[72] M.A.S. Azizi Samir, F. Alloin, A. Dufresne, Review of recent research into cellulosic whiskers, their properties and their application in nanocomposite field, Biomacromolecules. 6 (2) (2005) 612–626.
[73] K. Daicho, T. Saito, S. Fujisawa, A. Isogai, The crystallinity of nanocellulose: dispersion-induced disordering of the grain boundary in biologically structured cellulose, ACS Appl. Nano Mater. 1 (2018) 5774–5785.
[74] M.S. Rana, M.A. Rahim, M.P. Mosharraf, M.F.K. Tipu, J.A. Chowdhury, M. R. Haque, S. Kabir, M.S. Amran, A.A. Chowdhury, Morphological, spectroscopic and thermal analysis of cellulose nanocrystals extracted from waste jute fiber by acid hydrolysis, Polymers 15 (2023), 1530.
[75] B. Du, S.P.K. Jeepipalli, B. Xu, Critical review on alterations in physiochemical properties and molecular structure of natural polysaccharides upon ultrasonication, Ultrason. Sonochem. 90 (2022), 106170.
[76] J. Guo, X. Guo, S. Wang, Y. Yin, Effects of ultrasonic treatment during acid hydrolysis on the yield, particle size and structure of cellulose nanocrystals, Carbohydr. Polym. 135 (2016) 248–255.
[77] M. Girard, F. Bertrand, J.R. Tavares, M.-C. Heuzey, Rheological insights on the evolution of sonicated cellulose nanocrystal dispersions, Ultrason. Sonochem. 78 (2021), 105747.
[78] A.J. Sayyed, L.V. Mohite, N.A. Deshmukh, D.V. Pinjari, Effect of ultrasound treatment on swelling behavior of cellulose in aqueous N-methyl-morpholine-N-oxide solution, Ultrason. Sonochem. 49 (2018) 161–168.
[79] H.-Y. Kim, J.-A. Han, D.-K. Kweon, J.-D. Park, S.-T. Lim, Effect of ultrasonic treatments on nanoparticle preparation of acid-hydrolyzed waxy maize starch, Carbohydr. Polym. 93 (2) (2013) 582–588.
[80] Y. Tang, S. Yang, N. Zhang, J. Zhang, Preparation and characterization of nanocrystalline cellulose via low-intensity ultrasonic-assisted sulfuric acid hydrolysis, Cellulose 21 (1) (2014) 335–346.
[81] S.B.A. Hamid, S.K. Zain, R. Das, G. Centi, Synergic effect of tungstophosphoric acid and sonication for rapid synthesis of crystalline nanocellulose, Carbohydr. Polym. 138 (2016) 349–355.
[82] F. Azzam, L. Heux, J.-L. Putaux, B. Jean, Preparation by grafting onto, characterization, and properties of thermally responsive polymer-decorated cellulose nanocrystals, Biomacromolecules 11 (12) (2010) 3652–3659.
[83] S.J. Eichhorn, A. Dufresne, M. Aranguren, N.E. Marcovich, J.R. Capadona, S. J. Rowan, C. Weder, W. Thielemans, M. Roman, S. Renneckar, W. Gindl, S. Veigel, J. Keckes, H. Yano, K. Abe, M. Nogi, A.N. Nakagaito, A. Mangalam, J. Simonsen, A.S. Benight, A. Bismarck, L.A. Berglund, T. Peijs, Review: current international research into cellulose nanofibres and nanocomposites, J. Mater. Sci. 45 (2010) 1–33.
[84] B. Soni, E.B. Hassan, B. Mahmoud, Chemical isolation and characterization of different cellulose nanofibers from cotton stalks, Carbohydr. Polym. 134 (2015) 581–589.
[85] E.J. Foster, R.J. Moon, U.P. Agarwal, M.J. Bortner, J. Bras, S. Camarero-Espinosa, K.J. Chan, M.J.D. Clift, E.D. Cranston, S.J. Eichhorn, D.M. Fox, W.Y. Hamad, L. Heux, B. Jean, M. Korey, W. Nieh, K.J. Ong, M.S. Reid, S. Renneckar, R. Roberts, J.A. Shatkin, J. Simonsen, K. Stinson-Bagby, N. Wanasekara, J. Youngblood, Current characterization methods for cellulose nanomaterials, Chem. Soc. Rev. 47 (8) (2018) 2609–2679.
[86] Y. Peng, D.J. Gardner, Y. Han, Drying cellulose nanofibrils: in search of a suitable method, Cellulose. 19 (2012) 91–102.
[87] M.S. Reid, M. Villalobos, E.D. Cranston, Cellulose nanocrystal interactions probed by thin film swelling to predict dispersibility, Nanoscale. 8 (24) (2016) 12247–12257.
[88] J.S. Taurozzi, V.A. Hackley, M.R. Wiesner, Ultrasonic dispersion of nanoparticles for environmental, health and safety assessment – issues and recommendations, Nanotoxicology. 5 (4) (2011) 711–729.
[89] B. Zakani, S. Entezami, D. Grecov, H. Salem, A. Sedaghat, Effect of ultrasonication on lubrication performance of cellulose nano-crystalline (CNC) suspensions as green lubricants, Carbohydr. Polym. 282 (2022), 119084.
[90] T.G. Parton, R.M. Parker, G.T. van de Kerkhof, A. Narkevicius, J.S. Haataja, B. Frka-Petesic, S. Vignolini, Chiral self-assembly of cellulose nanocrystals is driven by crystallite bundles, Nat. Commun. 13 (2022) 2657.
[91] Q. Beuguel, J.R. Tavares, P.J. Carreau, M.-C. Heuzey, Ultrasonication of spray- and freeze-dried cellulose nanocrystals in water, J. Colloid Interface Sci. 516 (2018) 23–33.
[92] S. Shafiei-Sabet, W.Y. Hamad, S.G. Hatzikiriakos, Rheology of nanocrystalline cellulose aqueous suspensions, Langmuir. 28 (49) (2012) 17124–17133.
[93] H. Kargarzadeh, I. Ahmad, I. Abdullah, A. Dufresne, S.Y. Zainudin, R.M. Sheltami, Effects of hydrolysis conditions on the morphology, crystallinity, and thermal stability of cellulose nanocrystals extracted from kenaf bast fibers, Cellulose. 19 (3) (2012) 855–866.
[94] Y. Nishiyama, J. Sugiyama, H. Chanzy, P. Langan, Crystal structure and hydrogen bonding system in cellulose I_α from synchrotron X-ray and neutron fiber diffraction, J. Am. Chem. Soc. 125 (47) (2003) 14300–14306.
[95] S. Pradhan, J. Hedberg, E. Blomberg, S. Wold, I. Odnevall Wallinder, Effect of sonication on particle dispersion, administered dose and metal release of non-functionalized, non-inert metal nanoparticles, J. Nanopart. Res. 18 (2016) 285.
[96] I.M. Mahbubul, T.H. Chong, S.S. Khaleduzzaman, I.M. Shahrul, R. Saidur, B. D. Long, M.A. Amalina, Effect of ultrasonication duration on colloidal structure and viscosity of alumina-water nanofluid, Ind. Eng. Chem. Res. 53 (16) (2014) 6677–6684.
[97] I.M. Mahbubul, E.B. Elcioglu, R. Saidur, M.A. Amalina, Optimization of ultrasonication period for better dispersion and stability of TiO2–water nanofluid, Ultrason. Sonochem. 37 (2017) 360–367.
[98] J.-Y. Kim, D.-J. Park, S.-T. Lim, Fragmentation of waxy rice starch granules by enzymatic hydrolysis, Cereal Chem. 85 (2) (2008) 182–187.
[99] D. Pradhan, A.K. Jaiswal, S. Jaiswal, Emerging technologies for the production of nanocellulose from lignocellulosic biomass, Carbohydr. Polym. 285 (2022), 119258.
[100] R.M. dos Santos, W.P. Flauzino Neto, H.A. Silvério, D.F. Martins, N.O. Dantas, D. Pasquini, Cellulose nanocrystals from pineapple leaf, a new approach for the reuse of this agro-waste, Ind. Crops Prod. 50 (2013) 707–714.
[101] W.P. Flauzino Neto, H.A. Silvério, N.O. Dantas, D. Pasquini, Extraction and characterization of cellulose nanocrystals from agro-industrial residue – Soy hulls, Ind. Crops Prod. 42 (2013) 480–488.
[102] M. Nasir, R. Hashim, O. Sulaiman, M. Asim, Nanocellulose, in: Cellulose-Reinforced Nanofibre Composites, Elsevier, 2017, pp. 261–276.
[103] J. de Aguiar, T.J. Bondancia, P.I.C. Claro, L.H.C. Mattoso, C.S. Farinas, J. M. Marconcini, Enzymatic deconstruction of sugarcane bagasse and straw to obtain cellulose nanomaterials, ACS Sustain. Chem. Eng. 8 (5) (2020) 2287–2299.
[104] Z. Man, N. Muhammad, A. Sarwono, M.A. Bustam, M. Vignesh Kumar, S. Rafiq, Preparation of cellulose nanocrystals using an ionic liquid, J. Polym. Environ. 19 (3) (2011) 726–731.
[105] D. Trache, A.F. Tarchoun, M. Derradji, T.S. Hamidon, N. Masruchin, N. Brosse, M. H. Hussin, Nanocellulose: from fundamentals to advanced applications, Front. Chem. 8 (2020) 392.
[106] X. Luo, X. Wang, Preparation and characterization of nanocellulose fibers from NaOH/Urea pretreatment of oil palm fibers, BioResources. 12 (2017) 5826–5837.
[107] H. Du, X. Qian, The effects of acetate anion on cellulose dissolution and reaction in imidazolium ionic liquids, Carbohydr. Res. 346 (13) (2011) 1985–1990.
[108] R.S.A. Ribeiro, B.C. Pohlmann, V. Calado, N. Bojorge, N. Pereira, Production of nanocellulose by enzymatic hydrolysis: Trends and challenges, Eng. Life Sci. 19 (4) (2019) 279–291.

[109] P.B. Filson, B.E. Dawson-Andoh, D. Schwegler-Berry, Enzymatic-mediated production of cellulose nanocrystals from recycled pulp, Green Chem. 11 (2009) 1808.
[110] H.V. Lee, S.B.A. Hamid, S.K. Zain, Conversion of lignocellulosic biomass to nanocellulose: structure and chemical process, Sci. World J. 2014 (2014) 1–20.
[111] K.T. Chaka, Extraction of cellulose nanocrystals from agricultural by-products: a review, Green Chem. Lett. Rev. 15 (3) (2022) 582–597.
[112] J. Szadzińska, S.J. Kowalski, M. Stasiak, Microwave and ultrasound enhancement of convective drying of strawberries: Experimental and modeling efficiency, Int. J. Heat Mass Transf. 103 (2016) 1065–1074.
[113] H.V. Chuyen, M.H. Nguyen, P.D. Roach, J.B. Golding, S.E. Parks, Microwave-assisted extraction and ultrasound-assisted extraction for recovering carotenoids from Gac peel and their effects on antioxidant capacity of the extracts, Food Sci. Nutr. 6 (1) (2018) 189–196.
[114] R.C.N. Thilakarathna, L.F. Siow, T.-K. Tang, Y.Y. Lee, A review on application of ultrasound and ultrasound assisted technology for seed oil extraction, J. Food Sci. Technol. 60 (4) (2023) 1222–1236.
[115] Z.Z. Chowdhury, S.B.A. Hamid, Preparation and characterization of nanocrystalline cellulose using ultrasonication combined with a microwave-assisted pretreatment process, BioResources. 11 (2016) 3397–3415.
[116] H. Peng, H. Chen, Y. Qu, H. Li, J. Xu, Bioconversion of different sizes of microcrystalline cellulose pretreated by microwave irradiation with/without NaOH, Appl. Energy 117 (2014) 142–148.
[117] J. Gabhane, S.P.M. Prince William, A.N. Vaidya, K. Mahapatra, T. Chakrabarti, Influence of heating source on the efficacy of lignocellulosic pretreatment – A cellulosic ethanol perspective, Biomass Bioenergy 35 (1) (2011) 96–102.
[118] A. Dufresne, Nanocellulose: a new ageless bionanomaterial, Mater. Today. 16 (2013) 220–227.
[119] E. Wardhono, H. Wahyudi, S. Agustina, F. Oudet, M. Pinem, D. Clausse, K. Saleh, E. Guenin, Ultrasonic irradiation coupled with microwave treatment for eco-friendly process of isolating bacterial cellulose nanocrystals, Nanomaterials. 8 (2018) 859.
[120] X.Y. Tan, S.B. Abd Hamid, C.W. Lai, Preparation of high crystallinity cellulose nanocrystals (CNCs) by ionic liquid solvolysis, Biomass Bioenergy. 81 (2015) 584–591.
[121] G. Zhao, F. Wang, X. Lang, B. He, J. Li, X. Li, Facile one-pot fabrication of cellulose nanocrystals and enzymatic synthesis of its esterified derivative in mixed ionic liquids, RSC Adv. 7 (43) (2017) 27017–27023.
[122] Y. Ma, Q. Xia, Y. Liu, W. Chen, S. Liu, Q. Wang, Y. Liu, J. Li, H. Yu, Production of nanocellulose using hydrated deep eutectic solvent combined with ultrasonic treatment, ACS Omega 4 (5) (2019) 8539–8547.
[123] A.C.F. Louis, S. Venkatachalam, Energy efficient process for valorization of corn cob as a source for nanocrystalline cellulose and hemicellulose production, Int. J. Biol. Macromol. 163 (2020) 260–269.
[124] J. Senrayan, S. Venkatachalam, A short extraction time of vegetable oil from *Carica papaya* L. seeds using continuous ultrasound acoustic cavitation: Analysis of fatty acid profile and thermal behavior, J. Food Process Eng. 42 (2019), e12950.
[125] C. Sabater, V. Sabater, A. Olano, A. Montilla, N. Corzo, Ultrasound-assisted extraction of pectin from artichoke by-products. An artificial neural network approach to pectin characterisation, Food Hydrocoll. 98 (2020), 105238.
[126] H. Olivier-Bourbigou, L. Magna, D. Morvan, Ionic liquids and catalysis: Recent progress from knowledge to applications, Appl. Catal. A: Gen. 373 (2010) 1–56.
[127] T.P. Thuy Pham, C.-W. Cho, Y.-S. Yun, Environmental fate and toxicity of ionic liquids: A review, Water Res. 44 (2) (2010) 352–372.
[128] N.A. Samsudin, F.W. Low, Y. Yusoff, M. Shakeri, X.Y. Tan, C.W. Lai, N. Asim, C. S. Oon, K.S. Newaz, S.K. Tiong, N. Amin, Effect of temperature on synthesis of cellulose nanoparticles via ionic liquid hydrolysis process, J. Mol. Liq. 308 (2020), 113030.
[129] J. Lazko, T. Sénéchal, A. Bouchut, Y. Paint, L. Dangreau, A. Fradet, M. Tessier, J. M. Raquez, P. Dubois, Acid-free extraction of cellulose type I nanocrystals using Brønsted acid-type ionic liquids, Nanocomposites 2 (2) (2016) 65–75.
[130] B. Kosan, C. Michels, F. Meister, Dissolution and forming of cellulose with ionic liquids, Cellulose. 15 (1) (2008) 59–66.
[131] J. Han, C. Zhou, A.D. French, G. Han, Q. Wu, Characterization of cellulose II nanoparticles regenerated from 1-butyl-3-methylimidazolium chloride, Carbohydr. Polym. 94 (2) (2013) 773–781.
[132] J.H. Jordan, M.W. Easson, B.D. Condon, Cellulose hydrolysis using ionic liquids and inorganic acids under dilute conditions: morphological comparison of nanocellulose, RSC Adv. 10 (2020) 39413–39424.
[133] Z.Z. Chowdhury, R.R.R. Chandran, A. Jahan, K. Khalid, M.M. Rahman, M. Al-Amin, O. Akbarzadeh, I.A. Badruddin, T.M.Y. Khan, S. Kamangar, N.A.B. Hamizi, Y.A. Wahab, R.B. Johan, G.A. Adebisi, Extraction of cellulose nano-whiskers using ionic liquid-assisted ultra-sonication: optimization and mathematical modelling using box-behnken design, Symmetry. 11 (2019) 1148.
[134] S.B. Abd Hamid, Z.Z. Chowdhury, M.Z. Karim, Catalytic extraction of microcrystalline cellulose (MCC) from elaeis guineensis using central composite design (CCD), BioResources. 9 (2014) 7403–7426.
[135] M.d. Karim, Z. Chowdhury, S. Hamid, M.d. Ali, Statistical optimization for acid hydrolysis of microcrystalline cellulose and its physiochemical characterization by using metal ion catalyst, Materials. 7 (2014) 6982–6999.
[136] S.B. Abd Hamid, Z.Z. Chowdhury, M.Z. Karim, M.E. Ali, Catalytic isolation and physicochemical properties of nanocrystalline cellulose (NCC) using HCl-FeCl3 system combined with ultrasonication, BioResources. 11 (2016) 3840–3855.
[137] Z. Jin, S. Wang, J. Wang, MingXu Zhao, Effects of plasticization conditions on the structures and properties of cellulose packaging films from ionic liquid [BMIM]Cl, J. Appl. Polym. Sci. 125 (1) (2012) 704–709.
[138] D. Tian, Y. Han, C. Lu, X. Zhang, G. Yuan, Acidic ionic liquid as "quasi-homogeneous" catalyst for controllable synthesis of cellulose acetate, Carbohydr. Polym. 113 (2014) 83–90.
[139] W. Chen, H. Yu, Y. Liu, P. Chen, M. Zhang, Y. Hai, Individualization of cellulose nanofibers from wood using high-intensity ultrasonication combined with chemical pretreatments, Carbohydr. Polym. 83 (4) (2011) 1804–1811.
[140] P. Filson, B. Dawsonandoh, Sono-chemical preparation of cellulose nanocrystals from lignocellulose derived materials, Bioresour. Technol. 100 (7) (2009) 2259–2264.
[141] N. Johar, I. Ahmad, A. Dufresne, Extraction, preparation and characterization of cellulose fibres and nanocrystals from rice husk, Ind. Crops Prod. 37 (1) (2012) 93–99.
[142] E.L. Smith, A.P. Abbott, K.S. Ryder, Deep eutectic solvents (DESs) and their applications, Chem. Rev. 114 (21) (2014) 11060–11082.
[143] Q. Zhang, K. De Oliveira Vigier, S. Royer, F. Jérôme, Deep eutectic solvents: syntheses, properties and applications, Chem. Soc. Rev. 41 (2012) 7108.
[144] A.P. Abbott, D. Boothby, G. Capper, D.L. Davies, R.K. Rasheed, Deep eutectic solvents formed between choline chloride and carboxylic acids: versatile alternatives to ionic liquids, J. Am. Chem. Soc. 126 (2004) 9142–9147.
[145] Y. Liu, B. Guo, Q. Xia, J. Meng, W. Chen, S. Liu, Q. Wang, Y. Liu, J. Li, H. Yu, Efficient cleavage of strong hydrogen bonds in cotton by deep eutectic solvents and facile fabrication of cellulose nanocrystals in high yields, ACS Sustain. Chem. Eng. 5 (9) (2017) 7623–7631.
[146] M. Francisco, A. van den Bruinhorst, M.C. Kroon, New natural and renewable low transition temperature mixtures (LTTMs): screening as solvents for lignocellulosic biomass processing, Green Chem. 14 (2012) 2153.
[147] C. Alvarez-Vasco, R. Ma, M. Quintero, M. Guo, S. Geleynse, K.K. Ramasamy, M. Wolcott, X. Zhang, Unique low-molecular-weight lignin with high purity extracted from wood by deep eutectic solvents (DES): a source of lignin for valorization, Green Chem. 18 (2016) 5133–5141.
[148] E.E. Jaekel, J.A. Sirvio, M. Antonietti, S. Filonenko, One-step method for the preparation of cationic nanocellulose in reactive eutectic media, Green Chem. 23 (6) (2021) 2317–2323.
[149] T. Thiruganasambanthan, R.A. Ilyas, M.N.F. Norrrahim, T.S.M. Kumar, S. Siengchin, M.S.M. Misenan, M.A.A. Farid, N.M. Nurazzi, M.R.M. Asyraf, S.Z. S. Zakaria, M.R. Razman, Emerging developments on nanocellulose as liquid crystals: a biomimetic approach, Polymers. 14 (2022) 1546.
[150] L. Bai, L. Liu, M. Esquivel, B.L. Tardy, S. Huan, X. Niu, S. Liu, G. Yang, Y. Fan, O. J. Rojas, Nanochitin: chemistry, structure, assembly, and applications, Chem. Rev. 122 (2022) 11604–11674.
[151] Y.-D. He, Z.-L. Zhang, J. Xue, X.-H. Wang, F. Song, X.-L. Wang, L.-L. Zhu, Y.-Z. Wang, Biomimetic optical cellulose nanocrystal films with controllable iridescent color and environmental stimuli-responsive chromism, ACS Appl. Mater. Interfaces. 10 (6) (2018) 5805–5811.
[152] Hl. de Vries,, Rotatory power and other optical properties of certain liquid crystals, Acta Cryst. 4 (1951) 219–226.
[153] Q. Li, L. Green, N. Venkataraman, I. Shiyanovskaya, A. Khan, A. Urbas, J. W. Doane, Reversible photoswitchable axially chiral dopants with high helical twisting power, J. Am. Chem. Soc. 129 (43) (2007) 12908–12909.
[154] S. Beck, J. Bouchard, G. Chauve, R. Berry, Controlled production of patterns in iridescent solid films of cellulose nanocrystals, Cellulose. 20 (3) (2013) 1401–1411.
[155] P.-X. Wang, W.Y. Hamad, M.J. MacLachlan, Structure and transformation of tactoids in cellulose nanocrystal suspensions, Nat. Commun. 7 (2016) 11515.
[156] M. Esmaeili, K. George, G. Rezvan, N. Taheri-Qazvini, R. Zhang, M. Sadati, Capillary flow characterizations of chiral nematic cellulose nanocrystal suspensions, Langmuir. 38 (7) (2022) 2192–2204.
[157] Q.i. Chen, P. Liu, F. Nan, L. Zhou, J. Zhang, Tuning the iridescence of chiral nematic cellulose nanocrystal films with a vacuum-assisted self-assembly technique, Biomacromolecules. 15 (11) (2014) 4343–4350.
[158] F. Azzam, L. Heux, B. Jean, Adjustment of the chiral nematic phase properties of cellulose nanocrystals by polymer grafting, Langmuir. 32 (17) (2016) 4305–4312.
[159] E. Gicquel, J. Bras, C. Rey, J.-L. Putaux, F. Pignon, B. Jean, C. Martin, Impact of sonication on the rheological and colloidal properties of highly concentrated cellulose nanocrystal suspensions, Cellulose. 26 (13-14) (2019) 7619–7634.
[160] Y. Hu, N. Abidi, Distinct chiral nematic self-assembling behavior caused by different size-unified cellulose nanocrystals via a multistage separation, Langmuir. 32 (38) (2016) 9863–9872.
[161] M.S. Reid, M. Villalobos, E.D. Cranston, Benchmarking cellulose nanocrystals: from the laboratory to industrial production, Langmuir. 33 (2017) 1583–1598.
[162] A.S. Sonin, Inorganic lyotropic liquid crystals, J. Mater. Chem. 8 (1998) 2557–2574.
[163] G. Nyström, M. Arcari, J. Adamcik, I. Usov, R. Mezzenga, Nanocellulose fragmentation mechanisms and inversion of chirality from the single particle to the cholesteric phase, ACS Nano. 12 (6) (2018) 5141–5148.
[164] Q. Sun, V. Lutz-Bueno, J. Zhou, Y.e. Yuan, P. Fischer, Polymer induced liquid crystal phase behavior of cellulose nanocrystal dispersions, Nanoscale Adv. 4 (22) (2022) 4863–4870.
[165] X.M. Dong, T. Kimura, J.-F. Revol, D.G. Gray, Effects of ionic strength on the isotropic–chiral nematic phase transition of suspensions of cellulose crystallites, Langmuir. 12 (8) (1996) 2076–2082.
[166] Y. Sui, X. Li, W. Chang, H. Wan, W. Li, F. Yang, Z.-Z. Yu, Multi-responsive nanocomposite membranes of cellulose nanocrystals and poly(N-isopropyl

acrylamide) with tunable chiral nematic structures, Carbohydr. Polym. 232 (2020), 115778.
[167] J. Qin, N. Li, M. Jiang, L. Zong, H. Yang, Y. Yuan, J. Zhang, Ultrasonication pretreatment assisted rapid co-assembly of cellulose nanocrystal and metal ion for multifunctional application, Carbohydr. Polym. 277 (2022), 118829.
[168] X. Mu, D.G. Gray, Formation of chiral nematic films from cellulose nanocrystal suspensions is a two-stage process, Langmuir. 30 (31) (2014) 9256–9260.
[169] F. Nan, Q.i. Chen, P. Liu, S. Nagarajan, Y. Duan, J. Zhang, Iridescent graphene/cellulose nanocrystal film with water response and highly electrical conductivity, RSC Adv. 6 (96) (2016) 93673–93679.
[170] B.L. Tardy, J.J. Richardson, L.G. Greca, J. Guo, J. Bras, O.J. Rojas, Advancing bio-based materials for sustainable solutions to food packaging, Nat. Sustain. 6 (2023) 360–367.